Journal of Petroleum Geology, Vol. 47(4), October 2024, pp 395-430

STRATIGRAPHY AND DIAGENESIS OF THE THAMAMA-B RESERVOIR ZONE AND ITS SURROUNDING DENSE ZONES IN ABU DHABI OILFIELDS AND EQUIVALENT OMAN OUTCROPS

S. N. Ehrenberg[1]*, J. E. Neilson[2], E. Gomez-Rivas[3], N. H. Oxtoby[4], I.S.A.J. Jayachandran[5], Q. Adlan[6] and V. C. Vahrenkamp[7]

We review published studies characterizing the Thamama-B reservoir zone in the upper Kharaib Formation (late Barremian) in Abu Dhabi oilfields and at outcrops in Oman. Available data for oxygen and carbon isotope compositions, fluid inclusion measurements, cement abundance and formation water composition are interpreted in terms of a paragenetic model for the Thamama-B in field F in Abu Dhabi where the interval is deeply buried. The present synthesis provides a useful basis for understanding and predicting reservoir quality in static models and undrilled prospects, as well as for planning promising directions for further research. The goals of this study were to summarize the geologic setting and petrology of the Thamama-B reservoir and its surrounding dense zones, and to examine how sedimentology, stratigraphy and diagenesis have interacted to control porosity and permeability. Results that may have useful applications for similar microporous limestone reservoirs in general include:

- *the depositional environments and stratigraphy of the subject strata;*
- *a model for how porosity variations result mainly from calcite cementation sourced from stylolites, with little dependence on lithofacies other than the localization of chemical compaction by depositional clay linked to sequence stratigraphy;*
- *the use of solidity (rock thickness with porosity removed) as a check on porosity creation by burial dissolution;*
- *observations linking high-permeability streaks with storm lag beds and fractures;*
- *the concept of strata being gradually buried through a relatively static salinity-stratified water column;*
- *integration of conventional and clumped stable-isotope data with petrologic observations to constrain the timing of porosity evolution.*

[1] Ehrenberg Geoconsulting, Sandnes, Norway.
[2] School of Geosciences, University of Aberdeen, King's College, Aberdeen AB24 3UE.
[3] Departament de Mineralogia, Petrologia i Geologia Aplicada, Facultat de Ciències de la Terra, Universitat de Barcelona, Martí i Franquès s/n, 08028, Barcelona, Spain.
[4] retired, 41 Oaken Lane, Claygate, Surrey KT10 0RG.
[5] Texas A & M University, College Station, Texas, USA.
[6] Research Centre for Geological Resources, National Research and Innovation Agency (BRIN), Bandung, Indonesia.
[7] Energy Research and Petroleum Engineering, Ali I. Al-Naimi Petroleum Engineering Research Center, King Abdullah University of Science and Technology, Thuwal, Kingdom of Saudi Arabia.

* author for correspondence, e-mail: 111sne@gmail.com

Key words microporous carbonates, reservoir quality, diagenesis, sequence stratigraphy, isotope geochemistry.

[Correction added on 27 October 2024, after first online publication: This article is now open access. The open access legal statement has been added to reflect the change.]

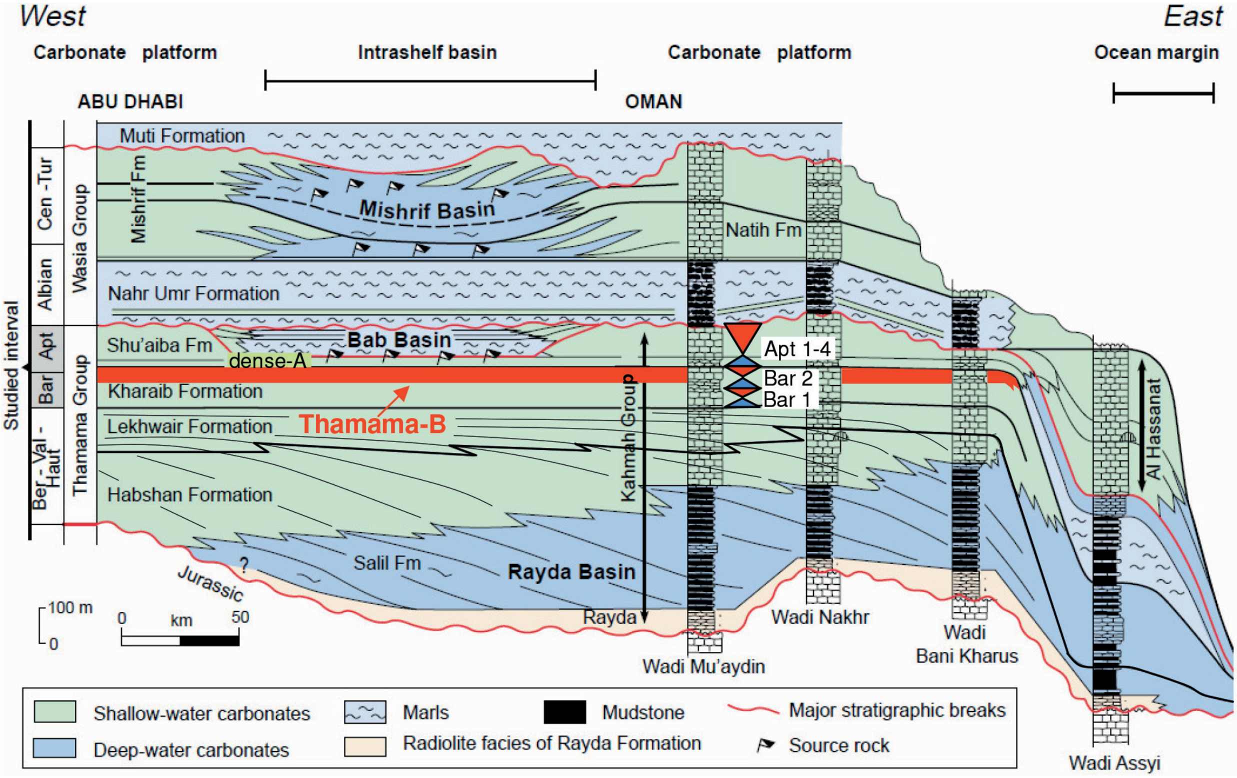

Fig. 1. Schematic regional stratigraphic cross-section through the Lower and middle Cretaceous in Abu Dhabi and Oman showing depositional geometries and lithostratigraphic nomenclature. Blue and red triangles are labeled with the 3rd-order sequence nomenclature of van Buchem *et al.* (2010a). Approximate location is shown in Fig. 3A. Modified from Figure 2 of van Buchem *et al.* (2002).

INTRODUCTION

The Thamama-B reservoir zone (Fig. 1) is the second of three mainly limestone reservoir intervals of Early Cretaceous age in the United Arab Emirates and the country's volumetrically most important oil-bearing stratigraphic unit (Carvalho *et al.*, 2011; Alsharhan *et al.*, 2014). The Thamama-B zone (also termed upper Kharib reservoir unit by Strohmenger *et al.*, 2006; Thamama II by Alsharhan, 1990; Kharaib-2 member by Gatel *et al.*, 2024) belongs to the late Barremian through earliest Aptian Kharaib Formation which is composed of intervals referred to (from the top) as the dense-A, zone B, dense-B, zone C and dense-C (Fig. 2) (Sharland *et al.*, 2001). Despite a large volume of scientific and industry-focused publications, a consistent understanding of the genesis of this important reservoir zone, its diagenetic alterations and the resulting distribution of reservoir properties is not well established. An overall goal of this review is to examine how sedimentology, stratigraphy and diagenesis have interacted to control the distribution of porosity and permeability in the unit both regionally and locally.

The Cretaceous was a time of widespread and recurrent formation of chalky, microporous limestones including the Thamama Group, the Mauddud Formation (Kuwait) and the Natih Formation (Oman); in areas outside the Arabian Plate, microporous limestones include the chalk in the North Sea of NW Europe, various carbonate formations in south Texas (Loucks and Bebout, 1984; Prezbindowski, 1985; Van Simaeys *et al.*, 2017), and the Cupido and Coahuila platforms in NE Mexico (Lehmann *et al.*, 2000). The Barremian-Aptian Urgonian limestones of SE France also have fundamental similarities to the Thamama strata (Cochard *et al.*, 2020; 2021; Tendil *et al.*, 2018; 2019). These microporous limestones include important reservoirs for oil and gas, and the present results may therefore have wide application. General take-aways from this study concern the way depositional clay is linked to sequence stratigraphy (especially falls in sea level); how this clay controls chemical compaction and resulting calcite cementation; the importance of storm lags and fractures in creating high-permeability streaks; the complementary use of fluid inclusion data, clumped-isotope data and conventional stable-isotope data for constraining paragenesis; and the effect of oil on inhibiting cementational porosity loss.

METHODS

The studied strata (Figs 1 and 2) are located in the subsurface of the United Arab Emirates, where the

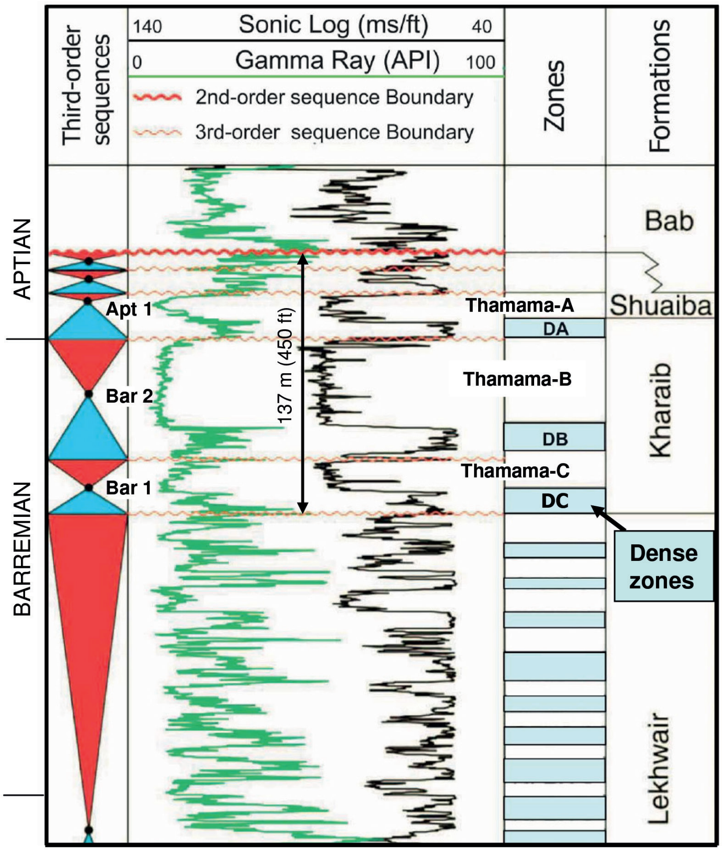

Fig. 2. Lithostratigraphic nomenclature relevant for the present study. Blue and red triangles are labeled with the sequence nomenclature of van Buchem *et al.* (2010a). Modified from Figure 3 of Strohmenger *et al.* (2006). Reprinted by permission of the AAPG whose permission is required for further use.

oilfields referred to in this paper are denoted by letter symbols (Fig. 3). Additional subsurface locations and outcrops in Oman from which data are available are shown by blue squares in Fig. 3. The Wadi Rahabah outcrop location is within the United Arab Emirates (Fig. 3). All data shown in the present compilation are from previously published sources but their review and synthesis provides a fresh overview. Values of $\delta^{13}C$ and $\delta^{18}O$ for rocks and minerals are reported here relative to the Vienna PDB scale (‰ VPDB), whereas $\delta^{18}O$ values for water are in ‰ SMOW. Analytical methods are described in the cited sources, except that whole-rock chemistry and stable-isotope methods are as described in Al Habsi *et al*., (2014). For the stable-isotope analyses, finely ground bulk-rock samples were reacted with 100% phosphoric acid in sealed vials for more than one hour at 90°C to dissolve all calcite and dolomite present. Textures are described in terms defined by Dunham (1962), Embry and Klovan (1971) and Lucia (1995).

The term "solidity" (modified from Baldwin and Butler, 1985) refers to stratigraphic thickness minus the average % porosity in the section, as determined from wireline logs (Ehrenberg *et al*., 2020a). Solidity is thus the solid mineral volume of a stratigraphic unit (zone or formation) in a particular location and provides a measure of unit thickness unaffected by mechanical compaction, but after any chemical changes, such as the export of material released by dissolution or the addition of cements from sources outside the unit.

PREVIOUS WORK

Basin evolution

The geological history of the study area in the UAE and Oman was described by Marzouk and El Sattar (1994), Ziegler (2001), Alsharhan *et al*. (2014), Ali *et al*. (2014) and Ali and Farid (2016). The Abu Dhabi Emirate is situated over the Rub Al Khali Basin, a NE-SW trending, intracratonic basin floored by the Upper Precambrian – Lower Cambrian Hormuz Salt. This area formed part of a >1000 km wide passive margin that developed along the SE margin of the Arabian Plate and accumulated carbonate strata in tropical latitudes under relative tectonic quiescence from Late Permian through middle Cretaceous time (Vahrenkamp *et al*., 2015).

The Early Cretaceous of the Arabian Plate bordering Neotethys saw a fundamental change in tectonic and depositional setting following plate-margin uplift and exposure which resulted in the Late Jurassic unconformity (Murris, 1980). Thermal subsidence at the end of the Jurassic (Tithonian) caused sudden collapse and retreat of the platform margin by some

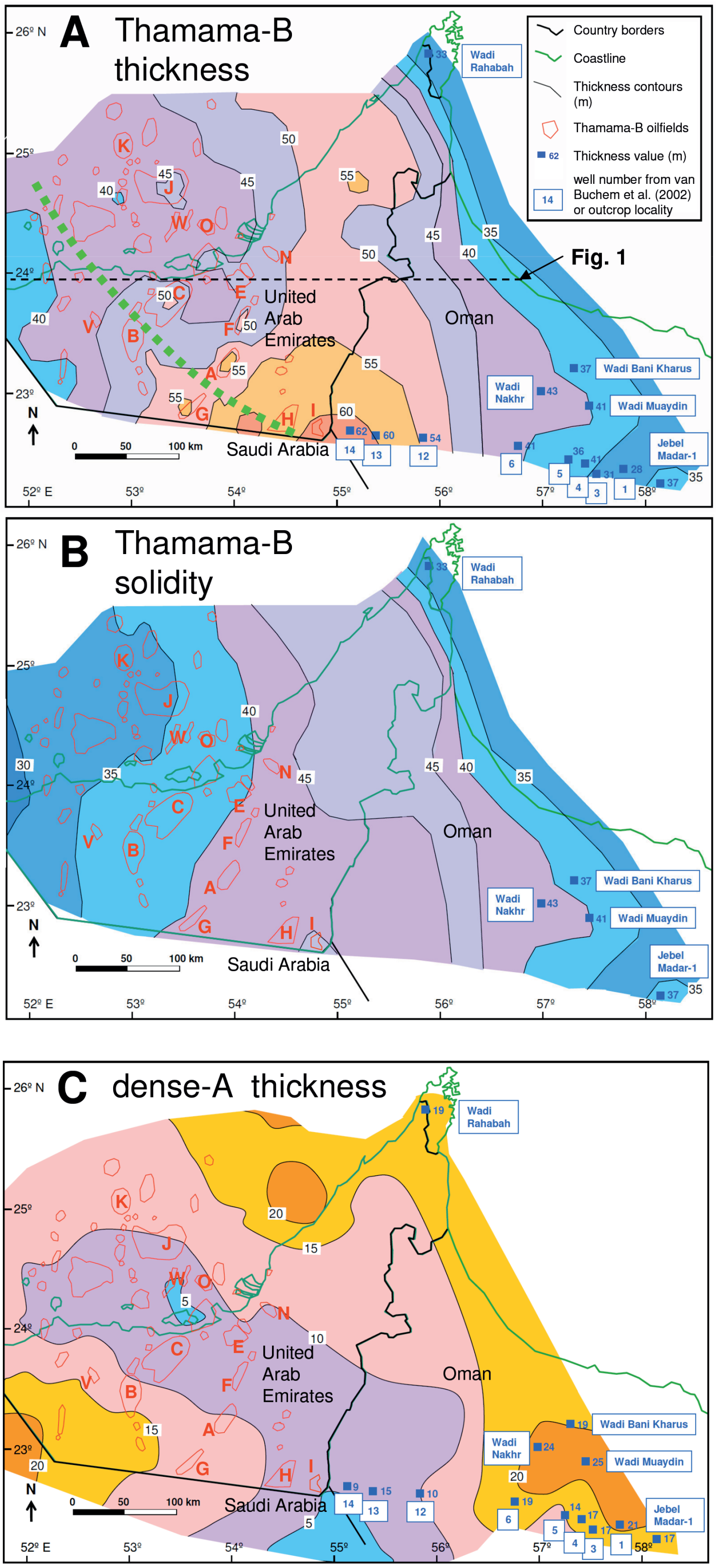

Fig. 3. Maps of Thamama-B (A) thickness and (B) solidity (thickness with porosity removed), and (C) dense-A thickness. Values are in metres. Red polygons are oilfield outlines. Fields discussed in text or figures are labeled with red letter symbols. Dashed black line in (A) shows the position of cross-section in Fig. 1. Dotted green line in (A) is the approximate axis of maximum thickness of sequence BAR 2 (Fig. 2) from Figure 6 of Vahrenkamp *et al.* (2015). Thickness values for locations marked by blue squares from van Buchem *et al.* (2002), except Wadi Rahabah from Alteneiji *et al.* (2024). (A) and B) modified from Fig. 17 of Ehrenberg *et al.* (2020a). Control points (shown in Fig. 15 of Ehrenberg *et al.*, 2020a) are abundant in the area of the oilfields, but include only the blue squares further east. (C) modified from Fig. 13 of Pierson *et al.* (2010), wherein the Abu Dhabi control points are shown.

600 km, creating the deep-marine Rayda Basin (Le Nindre *et al*., 2003; Rousseau *et al*., 2005; 2006; Fig. 1). Subsequently, starting during the late Tithonian, shallow-water platform-top facies (tidal-flat and lagoonal mudstones and wackestones) formed behind an eastward prograding platform margin composed of oolitic carbonate shoals (Dujoncquoy *et al*., 2018). In Abu Dhabi this latest Tithonian but mainly Berriasian to mid-Valanginian section is collectively called the Habshan Formation (Fig. 1; Sharland *et al*., 2001). The use of the term Habshan in Abu Dhabi contrasts with the Habshan of Oman, which is time-transgressive (Valanginian to Barremian) and describes the oolitic platform margin shoals that prograded eastward over slope deposits of the Salil Formation (Fig. 1; Razin *et al*., 2013; Dujoncquoy *et al*., 2018). Behind the prograding Habshan shoals, a giant relatively shallow lagoon developed which was filled with shallow -water sequences of alternating argillaceous and clean limestones of the Valanginian to Hauterivian Lekhwair Formation and the Barremian Kharaib Formation (Razin *et al*., 2013; Dujoncquoy *et al*., 2018). By the end of the early Barremian, the slopes and shoals had prograded all the way to the plate margin with several hundred metres of Lekhwair and Kharaib platform-top strata stacked behind the Habshan shoals (Grelaud *et al*, 2012; Fig. 1). Aggradation of the platform top continued through the Barremian with increasingly thicker cycles of the Kharaib Formation comprising the Thamama-C and Thamama-B zones (Fig. 2). Naming of the Thamama reservoir zones is derived from the sequence of penetration by the drill bit, starting with the Thamama-A which is part of the Shuaiba Formation and continuing through the Thamama-B and -C of the Kharaib Formation all the way down to the Valanginian Thamama-H, which is close to the bottom of the Lekhwair Formation (see Sharland *et al*, 2001, their Fig. 4.56).

Consequently, the Lekhwair and Kharaib Formations have remarkable "layer-cake" lateral continuity across an epeiric carbonate platform that covered most of the SE Arabian Plate. These strata are characterized by the repeated succession of (i) thin-bedded argillaceous limestones deposited during the initial flooding; (ii) wackestone/packstone layers with thin grainy caps characterizing the late transgressive unit; and (iii) fine- to coarse-grained units often enriched in larger bioclasts (rudists, microbial-algal-coated grains and other larger shallow-water carbonate components) of the highstand systems tract (Ehrenberg *et al*., 2018). The above basin evolution and the inner-ramp and lagoonal palaeogeography behind a Neotethys-facing shoal during the Barremian contrast with the outer- to mid- to inner-ramp progradational succession recently proposed for the Thamama-B strata by Gatel *et al*. (2024). During the following Aptian deposition of the Shuaiba Formation, the platform differentiated to form the intrashelf Bab Basin with surrounding shallow-water rudist build-ups (van Buchem *et al*., 2010a; Vahrenkamp, 2010; Vahrenkamp *et al*., 2015) (Fig. 1).

Following at least 50 million years of relative tectonic quiescence across this vast region, oblique compression caused by Late Cretaceous (Turonian-Campanian) obduction of the Semail Ophiolite onto the eastern margin of the Arabian Plate and, more importantly, the early Paleocene obduction of the Masairah Ophiolite in central Oman (Marquer *et al*, 1995; Schreurs and Immenhauser, 1999; Thomas and Heine, 2019), as well as compression associated with oblique collision of the Indian and Arabian Plates (Gomez-Rivas *et al*., 2014), produced strike-slip faulting in conjugate NW-SE and NE-SW directions (the Oman stress field of Marzouk and El Sattar, 1994, or the first Alpine phase of Loosveld *et al*., 1996). Most anticlinal structures of Abu Dhabi oilfields formed at this time, commonly aided in offshore Abu Dhabi areas by Hormuz Salt diapirism. After another period of relative quiescence, this was followed by collision of the African-Arabian Plate and the Eurasian Plate from the Eocene to the Pliocene (Madanipour *et al*., 2024), forming the Zagros fold-and-thrust belt (the second Alpine phase of Loosveld *et al*., 1996). In comparison, the Zagros stress field of Marzouk and El Sattar (1994) had less effect on the Lower Cretaceous strata of Abu Dhabi compared with the structures formed by the Late Cretaceous tectonics.

Hawas and Takezaki (1995) and Mohamed and Ennadi (1995) both concluded that most Abu Dhabi oil is sourced from Type II kerogen in the Upper Jurassic Diyab Formation, consisting of finely laminated, argillaceous lime mudstones which were deposited in an anoxic intrashelf basin. Diyab oil generation began in present-day onshore areas during the Campanian and in offshore areas during the Paleocene (Gumati, 1993). Alternatively, Taher (1997) proposed that oil was derived mainly by lateral migration from the Shuaiba Formation in the Bab Basin during the Eocene (as early as 50 Ma). More recently, Taher (2019) proposed that Thamama oil first accumulated in a palaeo-structure (underlying an area extending from Abu Dhabi city and about 100 km (62 miles) to the south), and then remigrated into the present-day field areas as the result of Late Cenozoic tilting. According to this model, the oil filled successive fields to spill-point along migration pathways out of the original palaeo-structure.

Sedimentology and stratigraphy

Thickness

The Thamama-B reservoir interval varies from 40 to 64 m (131-210 ft) in thickness in Abu Dhabi (Vahrenkamp *et al*., 2015; Fig. 3A). The strata are thickest in SE UAE and thin both westwards and towards the east, where correlative sections have been studied in outcrops (locations in Fig. 3; van Buchem *et al.*, 2002; Vaughan *et al.,* 2004; Immenhauser *et al*., 2004; Sattler *et al*., 2005). The seaward margin of the platform is seen in the eastern wadis of the Oman Mountains (Fig. 1; Hillgartner *et al.*, 2003; Hillgartner, 2010) and the northern U.A.E. near Khatt (Eilrich and Grötsch, 2003), but is not observed to the north of the Arabian Gulf, where the Kharaib Formation passes into the Gadvan Formation (Ziegler, 2001; van Buchem *et al*., 2010b). Figure 8 of Davies et al. (2002) shows that the Thamama-B continues to thin towards the NW, becoming 18-27 m (59-89 ft) thick in northern offshore Qatar. To the NW of Qatar towards Kuwait, the Kharaib Formation passes into the sandstones and shales of the upper Zubair Formation (Davies *et al.,* 2002; their Fig. 9).

Because compaction has reduced the thickness of the Thamama-B in many areas, trends in original depositional thickness are better displayed by variations in solidity (thickness with porosity removed; Fig. 3B), although the overall pattern is similar to the total thickness map of Fig. 3A. Porosity data are not available for the outcrop sections, but values are generally very low due to deep burial during plate-margin tectonism and are assumed to be zero for the solidity contouring. Although the porosity of these outcrop sections may have been enhanced in minor degree by telogenetic dissolution during tectonic uplift (possibly affecting only the present outcrop surfaces; Ehrenberg and Baek, 2019), this should not significantly affect the solidity thickness estimates. The wells from van Buchem *et al*. (2002; along the south edge of the map in Fig. 3A) were not included in the solidity contouring because total porosity values are not available for them.

Vahrenkamp *et al*. (2015; their Fig. 6) showed a map of the combined Thamama-B plus dense-B zones, which together constitute the Bar 2 third-order sequence of van Buchem *et al*. (2010a). Their map shows a broad NW-SE-oriented corridor of maximum thickness (roughly centered along the dotted green line in Fig. 3A), which they suggest corresponds to the axis of the future (Aptian) Bab Basin and resulted from far-field stresses extending from the Neotethys into the Arabian Plate.

The thickness of the dense-A zone (DA), which separates the Thamama-B from the overlying Shuaiba reservoir (Fig. 2), increases toward both the NE and SW from central Abu Dhabi (Fig. 3C). Pierson *et al*. (2010) and Vahrenkamp *et al*. (2015) showed similar maps of Hawar (dense-A) thickness and noted that the DA is thinner in central Abu Dhabi, along a NW-SE trend, where the Bab Basin would later develop. As the DA has porosity only slightly above zero, Fig. 3C is essentially equivalent to a solidity map.

Age constraints

Ages for the Barremian and Aptian strata of SE Arabia were determined by Schroeder *et al*. (2010) by calibration of orbitolinid biostratigraphy to Neotethyan ammonite zones (Fig. 4). The Thamama-B thus represents deposition during around 2 Ma of time in the late Barremian (orbitolinid zone 2a), occurring between the roughly 0.5 Ma-duration dense-B zone (DB: orbitolinid zone 1) and the 1.5 Ma-duration DA interval (upper part of orbitolinid zone 2). These results are supplemented by new taxa identified by Schlagintweit *et al*. (2024). The age of the upper Thamama-B has also been confirmed by strontium-isotope dates of 125.6 and 125.7 Ma from below the top contact in wells from two different oilfields (Figure 10a of Vahrenkamp, 2010 and Figure 3 in Strohmenger *et al*., 2010). Stratigraphic ages are further supported by correlation of carbon isotope profiles from Abu Dhabi well cores with European reference profiles (Vahrenkamp, 1996; 2010). Vahrenkamp *et al*. (2015; their Fig. 5) showed that strontium isotope calibration of ages indicates an overall subsidence rate of around 20 m/million years for Berriasian to Turonian strata in central Abu Dhabi.

Reservoir

As illustrated by the palaeogeographic diagrams in Figure 13 of van Buchem *et al*. (2002), both the Thamama-B and Thamama-C zones of the Kharaib Formation are viewed as having formed on an epeiric platform with a relatively flat, table-top geometry and little seaward slope. It is possible, however, that the individual cycles (sub-zones) comprising both zones were deposited by lateral progradation across the platform surface, as observed by Vaughan *et al*. (2004) in the upper portion of Thamama-B-equivalent outcrops in Wadi Rahabah (location shown in Fig. 3A). Droste (2010) interpreted the upper Thamama-B and overlying DA as paired prograding, open-marine and lagoonal facies belts, although others have viewed the top of the Thamama-B as an isochronal surface (van Buchem *et al*., 2010a). In any case, the platform-wide continuity of the Thamama-B sub-zones indicates that these layers must be bounded by isochronous surfaces.

Strohmenger *et al*. (2006) defined a system of 13 lithofacies in the Thamama-A, -B and -C reservoirs of field A in Abu Dhabi, as well as eight lithofacies in the intervening dense zones (*described below*), which has subsequently been the standard for core description within the Abu Dhabi National Oil Company. All the lithofacies names emphasize skeletal or peloid content, although both of these components are abundant in all lithofacies. Gatel *et al*. (2024) combined the lithofacies of Strohmenger *et al*. (2006) into 10 sedimentary facies to facilitate use of existing core descriptions from 295 wells in their statistical analyses. A simplification

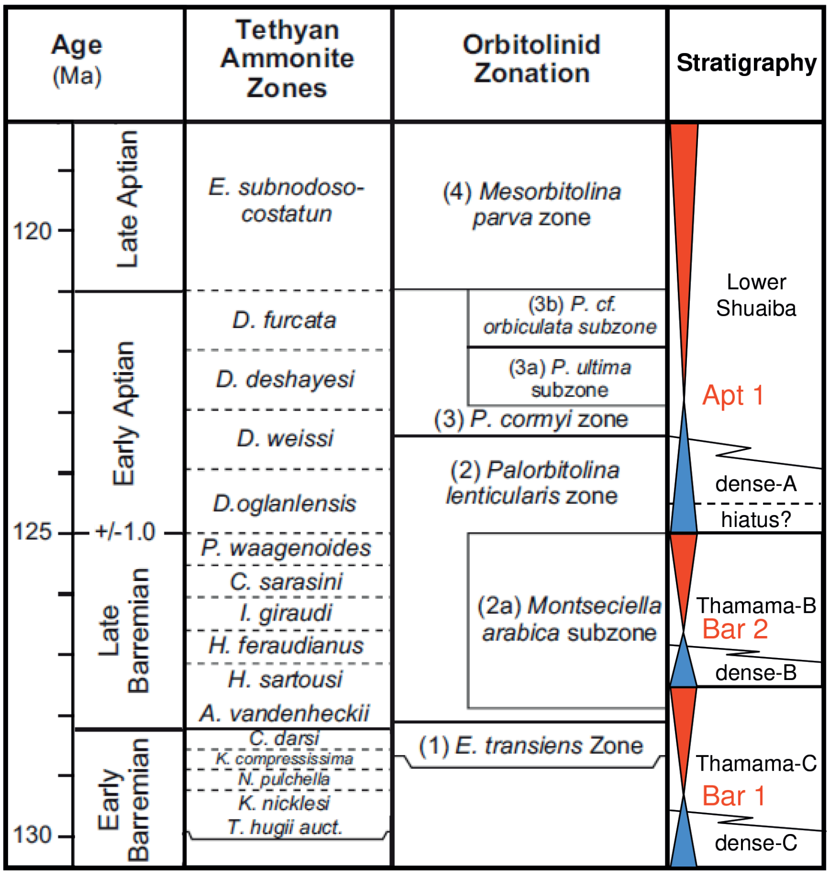

Fig. 4. Biostratigraphy and age interpretations for Thamama strata. Third-order sequences are labeled in red. Modified from Figure 10 of Schroeder *et al.* (2010).

of the Strohmenger *et al.* (2006) lithofacies used by Ehrenberg *et al.* (2018) for field F used only textures, but with rudstones and floatstones differentiated based on the dominant type of coarse clasts (rudist/bivalve, coated grain or intraclast). Tendil *et al.* (2021; 2022) used a system of seven "genetic elements", essentially combining lithofacies and corresponding depositional environments, for description of cores from the Lekhwair Formation and from an undisclosed Thamama stratigraphic level, respectively.

Based on observations of cores from fields F, C and J, the lower Thamama-B consists of mud-supported textures fluctuating around the border between mudstone and wackestone, gradually passing upwards into thoroughly bioturbated wackestone and mud-dominated packstone near the middle of the unit, and thence into the upper portion of coarser, grain-supported textures and finer beds that are more thinly and complexly interbedded. Alternations of these coarser and finer beds in the upper half of the unit probably reflect both platform-wide fluctuations in water depth and episodic storm activity that caused erosion and redistribution of low-relief organic build-ups (Ehrenberg *et al.*, 2018). Distinct hardgrounds and surfaces of subaerial exposure are not observed, but cemented intraclasts are common near the top of the zone, suggestive of intermittent seafloor cementation. Van Buchem *et al.* (2002) grouped these deposits in two facies associations. FA2a of the lower Thamama-B was suggested to represent open-marine conditions in the deep subtidal range above storm wave base. FA3 of the upper Thamama-B was viewed as representing shallow subtidal to intertidal settings. Higher GR activity and abundant clay-lined stylolites in the upper 3-4 m of the zone ("top interval" of Ehrenberg *et al.*, 2016) indicate episodic fine siliciclastic influx, possibly associated with numerous omission surfaces near the end of Thamama-B deposition in its latest regressional phase.

Dense zones

Intervals of argillaceous limestone with very low porosity in the Barremian and lowermost Aptian section of Abu Dhabi oilfields are referred to as "dense" because of their high bulk density values (Fig. 2). These strata were assigned by van Buchem *et al.* (2002) to "Facies Association 1b: Orbitolinid/calcareous algae -dominated argillaceous wackestone to packstones – interpreted as [having been deposited in] a mesotrophic environment". Orbitolinids are mainly large discoidal forms indicative of poor light penetration and abundant nutrient supply (Schroeder *et al.*, 2010). Pittet *et al.* (2002) suggested that biota of DA-equivalent strata in Oman indicate deposition in especially nutrient-rich conditions associated with influx of terrigenous fines. Another characteristic is ubiquitous pyritized ("blackened") bioclasts mixed with unaltered grains of the same taxa, suggestive of reworking of local anoxic enclaves.

Many authors have referred to the argillaceous limestones of the DA as the Hawar Member of the Kharaib Formation (Vahrenkamp, 1996; van Buchem *et al*., 2010a), but Davies *et al*. (2002) proposed that this is not appropriate because the Hawar Shale, as defined in Qatar, is dominantly siliciclastic. Their Figure 9 shows the Hawar Member of Qatar as passing northwestward into upper Zubair sandstone of Kuwait and pinching out eastward into upper Thamama-B limestone of offshore Abu Dhabi (field J), with the DA appearing at a somewhat higher stratigraphic level, but nevertheless containing the same K70 maximum flooding surface that they place at the top of the Hawar Shale in Qatar. Strohmenger *et al*. (2010) viewed the DA as a complete 3rd-order sequence, thus being isochronous across the epeiric platform; whereas Droste (2010) portrayed the Hawar Member (DA) in northern Oman as a lagoonal deposit of limited lateral extent and time-equivalent with the lowermost Shuaiba algal platform immediately to the west and north (his Figs 20 and 21).

Based on core descriptions from field F, the DA consists mainly of grain-supported textures and comprises 10-12 upward-coarsening cycles, many with burrowed firmground tops (Ehrenberg and Wu, 2019). In contrast, the DB consists of mudstone and subordinate wackestone, with cyclicity expressed by alternating high-GR intervals rich in dark, argillaceous laminations and thicker low-GR intervals with fewer dark layers (Ehrenberg and Wu, 2019). Wireline-logs, core descriptions and core photographs from other fields in Abu Dhabi and northern Oman indicate similar characteristics in both DA and DB. In Oman outcrops, both dense zones display cyclic alternations of wackestone and packstone textures (Pittet *et al*., 2002; van Buchem *et al*., 2002). As noted above, Strohmenger *et al*. (2006) defined eight dense-zone lithofacies: four termed "wispy-laminated, burrowed" and four termed "burrowed, bioturbated", with both sets of lithofacies including skeletal packstone; orbitolinid, skeletal packstone; orbitolinid, skeletal wackestone; and skeletal wackestone-mudstone. The rational for these is difficult to comprehend, however, as both DA and DB, at least in field F, are burrowed and bioturbated throughout, and also have orbitolinids and other skeletal components, as well as wispy laminations, common throughout and varying on decimetre to metre scale.

Both van Buchem *et al*. (2002) and Strohmenger *et al*. (2006) viewed the dense zones as shallow lagoonal deposits, and Droste (2010) referred to the Hawar Member (DA) as intertidal because of mud-cracks and root traces observed in Oman outcrops. In a Thamama-equivalent outcrop section in Wadi Rahabah, Alteneiji *et al*. (2024) described both DA and DB portions of the section as consisting mainly of lagoonal deposits (their lithofacies LF-12 and LF-13). Davies *et al*. (2002) and Steuber *et al*. (2022), however, suggested a deep-water setting for DA and DB. Gatel *et al*. (2024) did not include the DA in their work, but interpreted the DB as representing a deep basin environment.

Based on cores in field F, shallow water is indicated by the grain-supported, current-reworked textures of the DA, but deeper water, perhaps below storm wave base, seems likely for the mudstones of DB, in which the few bioclasts are limited to small, flat orbitolinids, *Choffatella,* echinoderm fragments and rare gastropods (Ehrenberg and Wu, 2019). Alternatively, the DB might be interpreted as representing a shallow lagoonal setting, well protected from current agitation, such as the present-day Florida Bay (Wanless and Tagett, 1989). Intense bioturbation throughout both dense zones indicates overall oxygen-rich conditions, despite the ubiquitous pyritized grains. Although DA and DB differ greatly in texture in field F, both intervals have similar ranges of bulk chemical composition (Ehrenberg and Wu, 2019), with cyclic fluctuations in clay content reaching a maximum in a thin condensed shale bed rich in glauconite and phosphate just below the top of DA and in two thin shale beds near the base of DB. A profile of bulk chemical analyses in the Thamama-equivalent outcrop section of Wadi Rahabah shows much lower siliciclastic content in DA and DB than in the subsurface section of field F, which Alteneiji *et al*. (2024) suggested to reflect the greater distance of this NE UAE locality (Fig. 3) from emergent areas that supplied siliciclastics to the carbonate platform.

Sequence stratigraphy

The distinct initial flooding and deepening marked by the DB and mud-dominated lower Thamama-B followed by an upward-shoaling trend of the grainy upper Thamama-B reservoir is regarded as a depositional sequence (Boichard *et al*., 1994) of roughly two million years' duration (Fig. 4), the Bar 2 sequence of van Buchem *et al*. (2010a), earlier designated as sequence II by Pittet *et al*. (2002). The Bar 2 sequence boundary (SB) is placed at the base of the DB (Fig. 2), which is regarded as the early transgressive systems tract (TST). The base of the overlying Apt 1 sequence occurs at the base of the DA (Fig. 2), also regarded as the early TST of that sequence.

Chronostratigraphic constraints are insufficient to confirm the 0.5 million-year hiatus posited at the top of the Thamama-B (Fig. 4) by van Buchem *et al*. (2010a) and in various earlier publications. Although commonly assumed, no actual evidence of subaerial exposure has been reported from Abu Dhabi well cores, either within or at the top of the Thamama-B zone. Warrlich *et al*. (2010) mentioned "karst features" at the top of the Thamama-B in Oman cores, and tidal-flat deposits with root traces, mudcracks and meteoric cements (calcite with negative O and C isotope excursions) have been reported in Thamama-B-equivalent outcrops in Oman (Huck *et al*., 2017; Pittet *et al*., 2002; Sattler *et al*., 2005) and at one horizon in Wadi Rahabah (which Alteneiji *et al*., 2024, used to divide the Thamama-B equivalent into two third-order sequences, an innovation apparently unique to that study). However, the presence of exposure in these eastern locations may reflect lesser accommodation near the platform margin rather than supporting emergence of the entire platform. Multiple omission surfaces are possible both within the upper 5-10 m of the Thamama-B and within the overlying DA, but actual evidence of emergence is elusive (Strohmenger *et al*., 2006; Ehrenberg *et al*., 2018). Nevertheless, the apparent lack of evidence for Thamama-B subaerial exposure in Abu Dhabi well cores does not necessarily mean that the platform surface never became emergent, as shown by the subtlety of such evidence along the top surface of the lower Shuaiba Formation where profound emergence is incontrovertible (Rameil *et al*., 2012).

Fourth-order cycles within the Thamama-B zone correspond with the seven main sub-zones used for production operations (I-VI in Fig. 5B), the boundaries of which are defined by subtle dips in porosity-log profiles and minor increases (peaks) in the GR log (Grötsch *et al*., 1998; Strohmenger *et al*., 2006). These boundaries result from thin (approximately 1-2 m; 3-6 ft) intervals of increased stylolite frequency, which correlate over tens to hundreds of kilometres (see Gatel *et al*., 2024, their Fig. 4b), apparently marking minor falls in sea level associated with increased clay influx across the platform. The increased clay content in these thin intervals is interpreted as having initiated stylolitization and local cementation as burial progressed (Koepnick, 1987; Ehrenberg *et al*., 2018), following the well-established relationship by which clay acts to localize and promote stylolitic dissolution (Aharonov and Katsman, 2009; Ehrenberg, 2022; Wang *et al*., 2023).

Additional clay-delimited (stylolite-bounded) cycles of 4th and smaller orders are likely present within several metres of the top and base of the Thamama-B, marked by reduced porosity and moderate GR peaks, as described by Ehrenberg *et al*. (2016; 2018), as well as within both dense zones (Ehrenberg and Wu, 2019). Frequent textural variations within the upper Thamama-B, commonly characterized by coarser beds overlying sharp, erosive bases with *Glossifungites*, may be either higher-order cycles (Eberli *et al*., 2001) or storm deposits (Ehrenberg *et al*., 2018).

Reservoir quality and diagenesis

Porosity data

Many publications show Thamama-B porosity profiles from individual fields in Abu Dhabi (Fig. 3). These include field J (Fox and Brown, 1968; Hassan *et al*., 1979; Alsharhan, 1990; Arab, 1991; Azer and Toland, 1993; Arab *et al*., 1994; Saotome *et al*., 2000), field A (Johnson and Budd, 1975; Koepnick, 1987; Alsharhan, 1993a; Grötsch *et al*., 1998; Alsharhan and Sadd, 2000; Melville *et al*., 2004; Strohmenger *et al*., 2006; Al-Mansoori *et al*., 2008), field F (Oswald *et al*., 1995; Alsharhan and Sadd, 2000; Al-Mansoori *et al*., 2008; Ehrenberg *et al*., 2016; Paganoni *et al*., 2016), field C (Harris *et al*., 1968; Alsharhan and Sadd, 2000; Al-Mansoori *et al*., 2008; Ehrenberg *et al*., 2020b), field B (Alsharhan, 1985; 1993b), fields O and K (Azer and Toland, 1993), field E (Alsharhan and Sadd, 2000), field I (Alsharhan and Sadd, 2000), field N (Abou Zeid and El Bishlawy, 1989) and various other fields (van Buchem *et al*., 2002; Al-Mansoori *et al*., 2008; Tendil *et al*., 2022). These profiles are all fairly similar to the examples in Fig. 5, with an overall blocky, high-porosity profile interrupted by thin intervals of decreased porosity at subzone tops and thicker intervals of decreased porosity in the uppermost and lowermost 5-10 m of the zone. There is also a more subtle trend of decreasing porosity and permeability from the grain-supported facies of the upper half of the zone to the mud-supported facies of the lower half.

It is simplest to consider the effects of burial on reservoir porosity in terms of depth, but temperature and especially temperature history ("thermal exposure") may be more meaningful scales for measuring changes in cementation and porosity (Schmoker, 1984; Walderhaug, 1996). In basins such as that underlying Abu Dhabi where strata were gradually buried to their maximum depth, present-day temperature should be roughly proportional to thermal exposure and can serve as a basis for comparison. The general trend of decreasing average porosity with depth for the Thamama-B in different fields in Abu Dhabi is similar to the well-known trend for South Florida carbonates (Fig. 6), which were also buried gradually to their present-day maximum depth (Schmoker and Halley, 1982). South Florida has a much cooler geotherm than Abu Dhabi, however −18 ºC/km versus 36 ºC/km (Ehrenberg *et al*., 2020a; their Fig. 5), respectively − and thus porosity loss in South Florida has been much greater than the Thamama-B trend when compared in terms of present-day temperatures (Fig. 6). The question arises, therefore, as to whether overburden stress (depth) or thermal exposure is the more important basis for comparison (Ehrenberg, 2022).

Permeability data

Many authors have documented the overwhelming

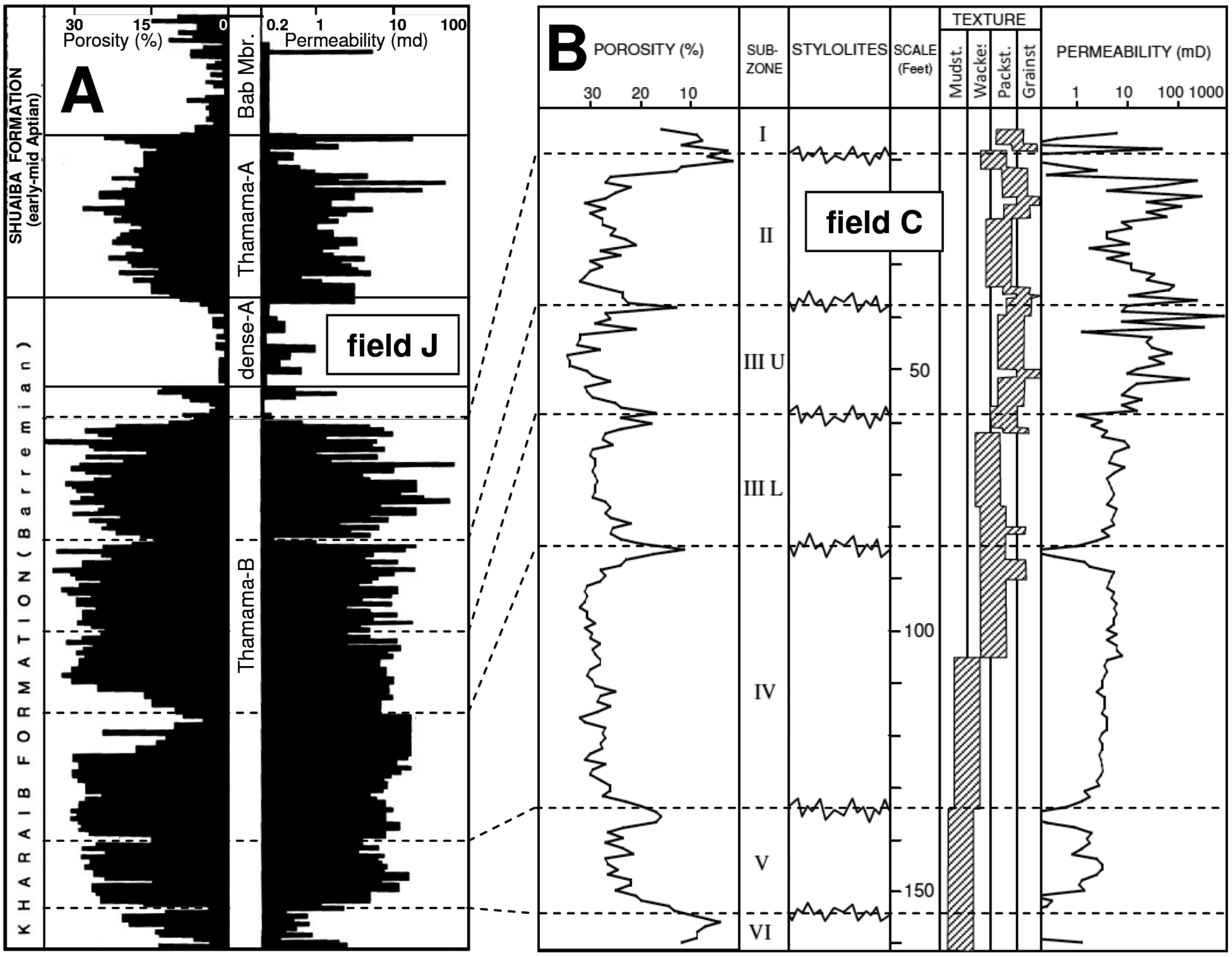

Fig. 5. Profiles of porosity and permeability. Dashed lines show the platform-wide correlation of the six Thamama-B sub-zone tops, defined by thin intervals of lower porosity, reflecting greater frequency of stylolites that caused local increase in calcite cementation. (A) Reservoirs and dense zones of field J. Modified from Figure 4 of Alsharhan (1990). No vertical scale was given in the original figure, but Thamama-B thickness is roughly 45 m (Fig. 3A). (B) Thamama-B reservoir of field C, where Thamama-B thickness is 47 m. Drafted following Figure 4 of Harris *et al.* (1968).

dominance of microporosity in Thamama-B reservoirs (Budd, 1989; Grotsch *et al.*, 1998; Vahrenkamp *et al.*, 2014; Morad *et al.*, 2016; Morad *et al.*, 2018; Ehrenberg, 2019; Ehrenberg *et al.*, 2020b). This results in low overall permeability-for-given-porosity (Lucia class 3 field), but the trend for average well values (Fig. 7) lies somewhat above the trend for microporosity-dominated limestones (Fullmer *et al.*, 2014; Kaczmarec *et al.*, 2015). Interestingly, although wells with Thamama-B oil zones have generally higher porosity than water-zone wells, both fluid zones lie along the same porosity-$\log_{10}$(permeability) trend (Fig. 7).

Texture appears to have had only a subtle influence on Thamama-B permeability. Based on the example of field F, increasing grain content and grain size results in a systematic but minor increase in the trend of $\log_{10}$(permeability)-porosity correlation, although the slope of the trend remains roughly constant (Fig. 8). Thus, grainstone and grain-dominated textures (Fig. 8A) tend to have higher permeability-for-given-porosity than grain-supported, mud-dominated textures (Fig. 8B), which are in turn higher than mud-supported textures (Fig. 8C). Increasing grain size (floatstone and rudstone versus packstone) also tends to correlate with higher permeability-for-given-porosity (Fig. 8A, B). The regression trends shown in Fig. 8 exclude samples with anomalously high permeability at low porosity (shown by blue squares with grey shading), which are suspected to be plugs containing fractures. The regression trends, however, include a subordinate population of "hi-K" samples having high permeability values judged likely to be in-place characteristics of the reservoir rather than artifacts of plug fracturing (shown by blue squares with no shading in Fig. 8). Petrographic observation shows these samples to contain either coarse grains with high contents of atypically large macropores or tensional fractures perpendicular stylolites (Ehrenberg, 2019).

The above hi-K samples likely correspond with the "high permeability streaks" (HKS) occurring as thin

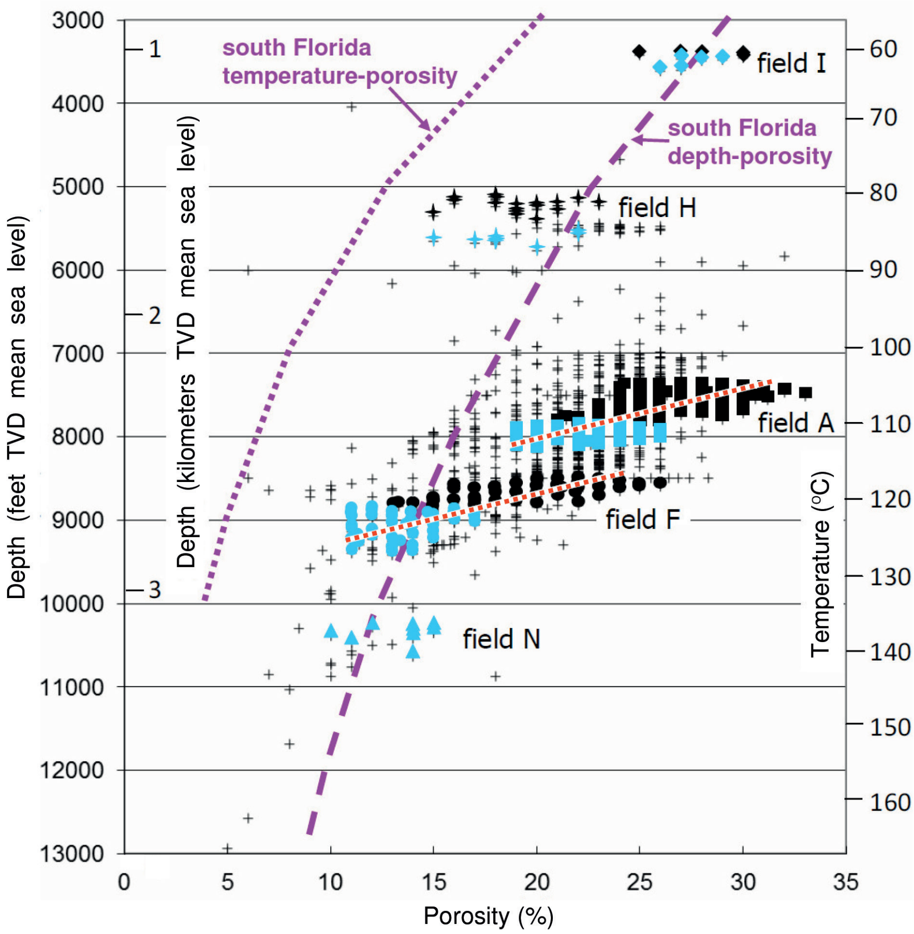

Fig. 6. Depth and temperature vs. average wireline-log porosity of entire Thamama-B zone in Abu Dhabi wells. Larger symbols are from the five labeled fields - colour indicates wells with average depth above (black) and below (blue) free-water level. Small black crosses are wells from other fields. Dotted red lines are average trends for fields A and F. Purple curves are trends of South Florida carbonates (Schmoker and Halley, 1982) plotted at equivalent depths (dashed) and temperature (dotted). Modified from Figures 8 and 12 of Ehrenberg *et al.* (2020a).

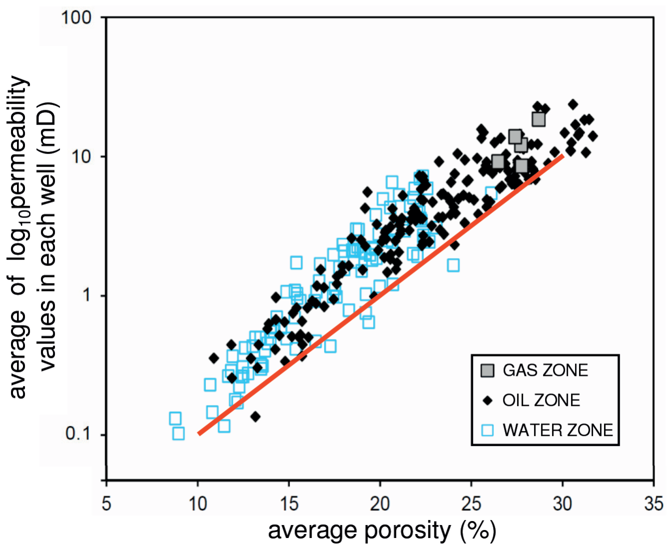

Fig. 7. Arithmetic average permeability vs. average porosity of RCA plug analyses. Each point represents the average value for the entire Thamama-B zone in one well. Symbols indicate wells with average depth above (black) and below (blue) free-water level and wells in one field above gas-water contact (grey). Red line is the trend for microporosity dominated limestones (microporosity = 80% or more of total porosity) from Fullmer *et al.* (2014). Modified from Figure 7 of Ehrenberg *et al.* (2020b).

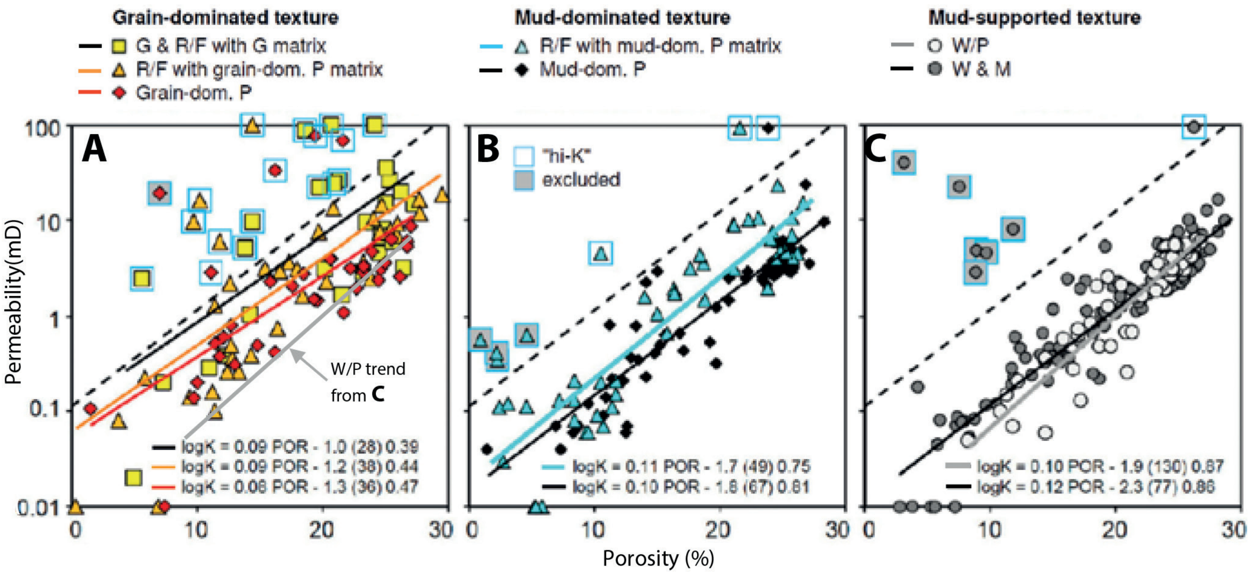

Fig. 8. Permeability vs. porosity of RCA plug analyses for samples with corresponding thin sections from field F, grouped by texture (R = rudstone; F = floatstone; G = grainstone; P = packstone; W = wackestone; M = mudstone). Dashed lines show the trend one log(permeability) unit above the W & M trend, used as the boundary above which samples are defined as "hi-K" (high permeability) or are excluded because of suspected plug damage. Solid diagonal lines are least-squares fits to the undamaged samples of each texture group. Equations for each line are listed as "logK" ($\log_{10}$(permeability) mD) = [factor] times "POR" (porosity %) minus [intercept] followed by number of samples in parentheses and the r-squared value. Regressions include all samples except those marked "excluded". Modified from Figure 10 of Ehrenberg (2019). Reprinted by permission of the AAPG whose permission is required for further use.

(0.15-0.75 m; 0.5-2.5 ft) beds in the upper Thamama-B of field J (Saotome *et al*., 2000; Ottinger *et al*., 2012; Skene *et al*., 2014) and field C (Khan *et al*., 2021). These studies link the HKS with coarse, mud-lean storm beds deposited in relatively low areas of the sea floor between tidal ridges. Reservoir quality is variably enhanced by dissolution or, in flank wells, degraded by cementation. In addition, fractures (Bushara and Arab, 1998; Shekhar *et al*., 2019) and dolomitized burrows (Shekhar *et al*., 2017) are also locally important causes of HKS which contributed to early break-through during water flooding in field J.

It is possible to examine the overall effects of texture on permeability by comparing routine core analysis (RCA) data from the upper and lower parts of the Thamama-B zone. Macropores are common, but subordinate, in the upper, more grain-rich half of the reservoir, but are rare to absent throughout the lower part. Within individual fields, the upper and lower Thamama-B both display similar wide ranges of porosity (example shown in Fig. 9), but the upper half of the reservoir shows greater dispersion with many more "hi-K" values (permeability above the dashed line of Fig. 9). Similar examples comparing RCA data from upper versus lower Thamama-B are shown for three other large oilfields in Figure 9 of Ehrenberg *et al*. (2020b). Comparison with Figure 3C of Fullmer *et al*. (2019) shows that the hi-K samples must be those in which macroporosity is substantially >20% of total porosity. Most of the Thamama-B zone, however, appears to have >80% microporosity and should therefore have favorable characteristics of oil displacement and sweep efficiency (Fullmer *et al*., 2019).

Compilations of data from the above four large fields show that the hi-K samples are concentrated in particular areas of each field (Fig. 10A; Ehrenberg *et al.*, 2020b). Petrographic study of the hi-K samples from field F shows that these values are related to higher content of macropores in coarser, grain-rich textures (Ehrenberg, 2019). Similar results are reported for field C (Fig. 10B) and field J (Brantferger *et al*., 2012; Ottinger *et al*., 2012; Skene *et al*., 2014), where the high-permeability streaks are interpreted as coarse lags deposited by storms.

Cementation and dolomitization

As described by Paganoni et at. (2016), Morad *et al*. (2016) and Ehrenberg *et al*. (2016), calcite is by far the most abundant cement in the Thamama B limestones. Of the various morphologies present, the most abundant are blocky macrocement in larger pores and microcement within mud matrix and microporous grains, although actual volumes are impractical to estimate quantitatively and likely vary widely even between closely-adjacent samples. Dolomite is a widespread minor component occurring both as a replacement of calcite and as pore-filling cement.

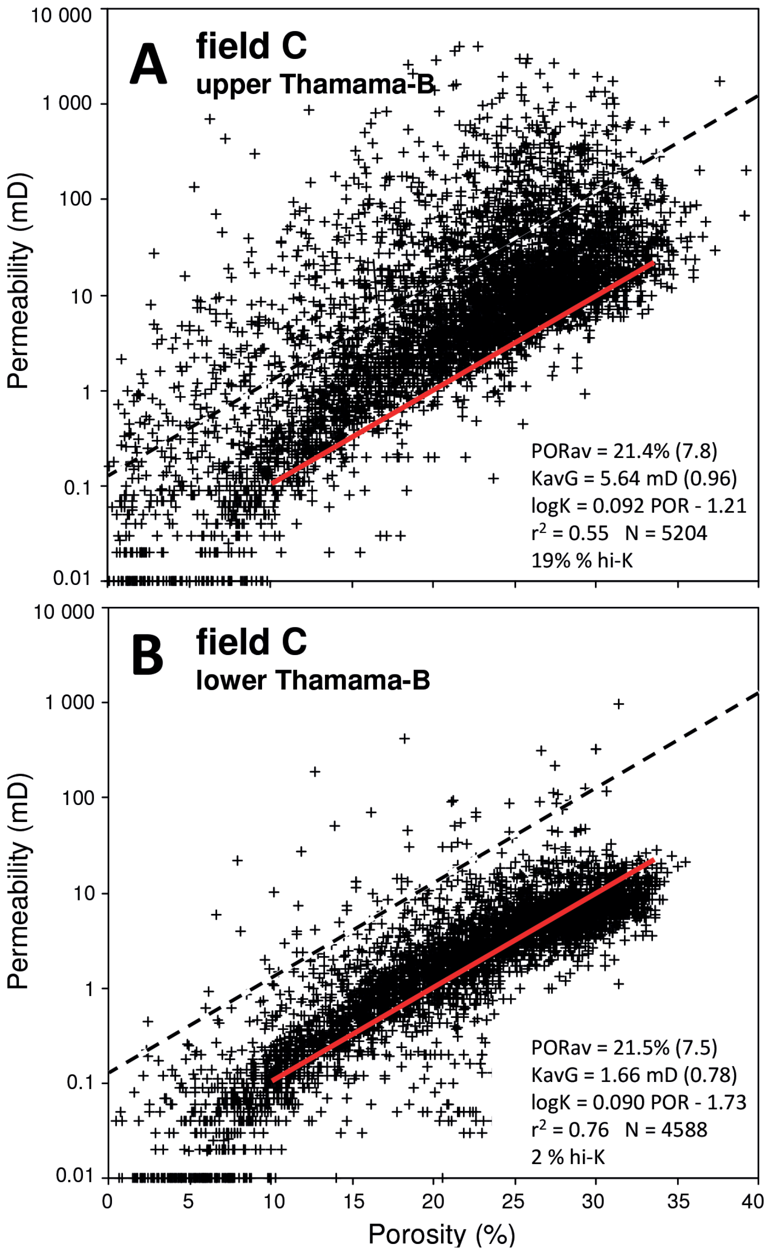

Fig. 9. Porosity vs. permeability for RCA data from field C, comparing (A) upper Thamama-B (sub-zones I, II, IIU, IIIL) and (B) lower Thamama-B (sub-zones IV, V, VI). Red line is the trend for microporosity-dominated limestones of Fullmer *et al.* (2014). Dashed line is equivalent to dashed line in Fig. 8 (one log unit above best fit to wackestone and mudstone data of Fig. 8C), above which samples are defined as "hi-K". Modified from Figure 9C, D of Ehrenberg *et al.* (2020b).

Both finely crystalline planar dolomite and more coarsely crystalline saddle dolomite are present, with many examples transitional between these types. Both are typically more abundant along stylolites and wispy dissolution seams, possibly reflecting reaction between ions released from clays and the carbonate ions released by chemical compaction. Halos of replacive saddle dolomite are commonly concentrated along the trailing side of the advancing segments of rectangular stylolites, and both saddle dolomite and calcite cement, as well as dickite, tend to fill tension fractures perpendicular to stylolite planes (Fig. 11). Exotic cements, including kaolin, sphalerite and fluorite of the type identified by Neilson and Oxtoby (2008), are typically present in minor amounts.

In general and in common with other Cretaceous carbonate reservoirs in the Arabian Plate (Ehrenberg *et al.*, 2008), dolomitization is minor in most Thamama-B fields, but a thin stratiform bed of high-permeability dolostone is present near the base of the Thamama-B zone in field J (Fig. 12A, B, F). Its geometry and geochemistry indicate formation shortly after deposition by diffusion of ions from seawater, followed by burial cementation that was inhibited on the structural crest by oil emplacement (Yamamoto *et al.*, 2018). A stratiform dolostone layer of similar thickness

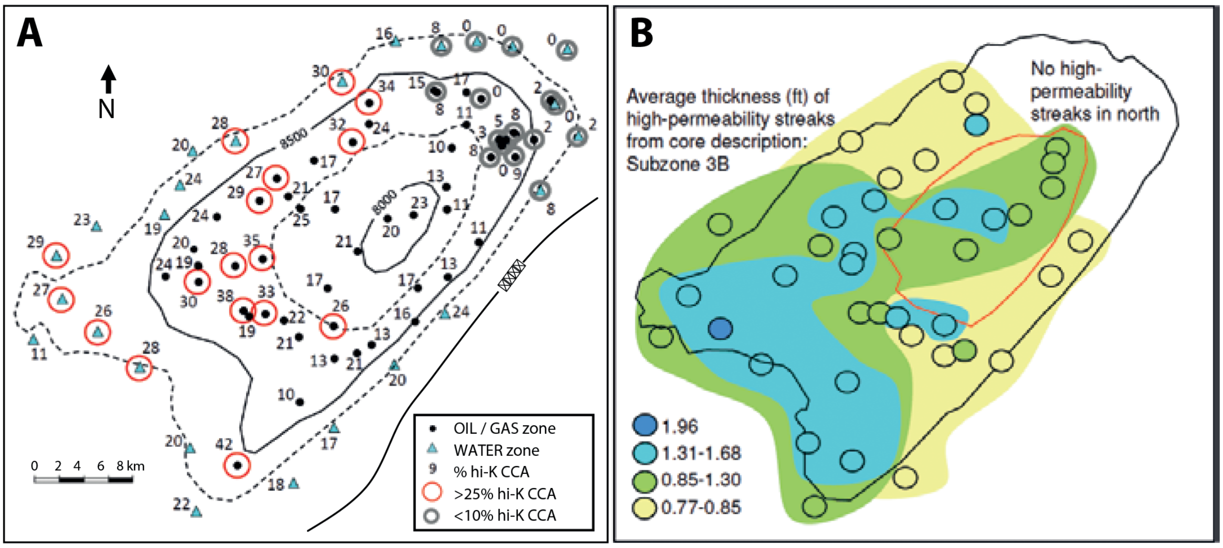

Fig. 10. (A) Distribution of "hi-K" sample abundances in field C. Numbers are % "hi-K" conventional core analysis (CCA) plugs (defined in Fig. 8) as percentage of the total number of CCA data in upper half of Thamama-B zone, excluding data with <8% porosity. Inner symbols indicate wells with average depth above (black) and below (blue) free-water level. Circles highlight wells having higher (RED) and lower (GRAY) ranges of % hi-k samples. Solid lines are top-Thamama-B structural contours (ft TVDss). Dashed lines are free-water level and gas/oil contact. Modified from Figure 12 of Ehrenberg *et al.* (2020b). (B) Average thickness of high-permeability streaks (mainly thin beds of grainstone and rudstone deposited by storm events) in subzone 3B of field C (equivalent to subzone IIIL in Fig. 6B). Black and red lines are oil/water contact and gas/oil contact, respectively. Symbol colors indicate thickness ranges. Redrafted from Figure 8 of Khan *et al.* (2021).

is also present 2 m below the top of the equivalent outcrop section in Wadi Rahabah in the NE UAE (Fig. 12C, D, E) (location in Fig. 3). Alteneiji *et al.* (2024) describe this layer as consisting of de-dolomite, but thin sections from a series of three samples collected near the base, centre and top of the layer by the senior author show common calcite cement and allochems, but no sign of de-dolomite texture, although both dolomite and calcite in the central sample show late dissolution (Fig. 12E). Five thin (<0.5 m) de-dolomite beds are also reported in the underlying Lekhwar Formation and Thamama-C equivalent in outcrops of Jebel Madar, Oman (Huck *et al.*, 2017). Field J also contains abundant dolomitized burrows in the middle portion of the reservoir: "randomly oriented and distributed features on a scale of cm to 10s of cm" that "tend to be filled with grainer limestone having higher permeability than the enclosing wackestone and packstone" (Al-Neyadi *et al.*, 2012; Shekhar *et al.*, 2017). Dolomitized burrow networks also occur in the lower part of the Thamama-B-equivalent section in Wadi Rahabah, as noted by Alteneiji *et al.* (2024). Selective dolomitizsation of burrows in shallow-marine carbonates has been found to result from concentration of echinoderm fragments, consisting of high-magnesium calcite (Liu *et al.*, 2024).

Fluid inclusion measurements
Primary fluid inclusions in calcite cements from Thamama-B cores in Abu Dhabi field F have salinities ranging from 2.5 to 24% NaCl-equivalent and homogenization temperatures of 70-140 ºC (Fig. 13). These data are from Morad *et al.* (2019), but very similar results were also found by Jayachandran (2017). Similar ranges were reported by Neilson *et al.* (1998) from unspecified fields. Morad *et al.* (2019) interpreted these ranges as reflecting gradual cementation during progressive burial. The overall less saline and somewhat lower temperature range of the fluid inclusions from crestal wells in field F is consistent with oil having retarded later stages of cement growth. In both water and oil zones, the fluid inclusions in cements located along stylolites tend to have higher salinities and homogenization temperatures than inclusions more distant from stylolites (Fig. 13). Morad *et al.* (2019) suggested that this indicates flux of basinal brines entering the limestones along stylolites.

Carbon and oxygen isotope analyses
Stable isotope analyses from the Thamama-B and its surrounding dense zones are interpreted below in relation to an extensive framework of previous work that is briefly summarized as a basis for the following review. Carbon isotope values of bulk-carbonate and cement samples from Cretaceous cores and outcrops in SE Arabia mainly record variations in seawater composition at the time of deposition, providing a useful tool for stratigraphic correlation (Vahrenkamp, 1996; 2010; Droste, 2010; Huck *et al.*, 2017; Strohmenger *et al.*, 2010). Locally, however, negative excursions from

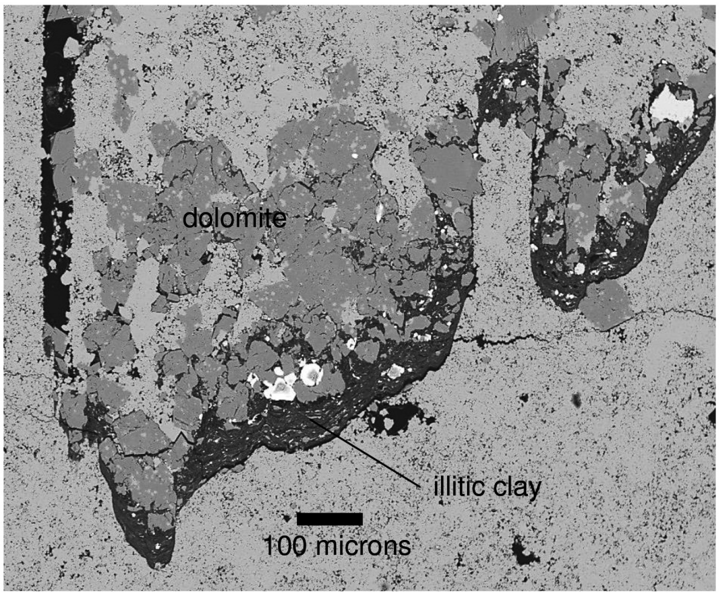

Fig. 11. Back-scattered electron image of a polished thin section with a rectangular stylolite in field F. Brightness is proportional to average atomic number. The main, light grey areas are calcite. Bright crystals at lower center are phosphate that has grown around cores of dolomite. The roughly bedding-parallel (semi-horizontal) segments are lined with illitic clay and have dolomite concentrated along the trailing side. The vertical segment at left (a strike-slip offset) has opened in response to tensile stress and is partly filled by euhedral calcite and dolomite crystals surrounded by pore space (black). Well F4, core depth 9633 ft (top of sub-unit IIIL). From Ehrenberg *et al.* (2016).

seawater values immediately underlying discontinuity surfaces provide evidence of soil development during subaerial exposure (Immenhauser *et al*., 1999; 2000; Rameil *et al*., 2012), and rare positive excursions are seen as reflecting methanogenesis (Raven and Dickson, 2007). Neither of these latter effects, however, have been reported in Thamama-B studies.

Oxygen isotope variations in carbonate strata can also partly reflect seawater composition, which is estimated to have been around -2‰ SMOW in the Early Cretaceous (Lohmann, 1988; Veizer *et al*., 1999), as well as seawater temperature and the effects of diagenetic re-equilibration of depositional components and precipitation of cements. As the resulting $\delta^{18}O$ of calcite depends on both equilibration temperature and the isotopic composition of the water involved, the range of values of one of these two variables must be assumed or independently measured in order to constrain the other (Lohmann, 1988). Thus, oxygen isotope values can reflect a complex combination of varying temperatures and formation water compositions from deposition through to the present-day maximum burial depth. The three variables are related according to the equation of Kim and O'Neill (1997), which can be simplified as:

$$(1)\quad T[°C] = 17880 / (\delta^{18}O_{calcite}[‰PDB] * 1.03086 + 62 - \delta^{18}O_{water}[‰SMOW]) - 273.15$$

Using this equation, the average temperature of equilibration of calcite in a sample can be calculated by assuming an average value for the oxygen isotope composition for the waters involved. Equation 1 can be rearranged as follows to solve for the oxygen isotope composition of the calcite for given temperature and water composition:

$$(2)\quad \delta^{18}O_{calcite}[‰PDB] = (17780/ (T[°C] + 273.15) - 62 + \delta^{18}O_{water}[‰SMOW]) / 1.03086$$

Published analyses of C and O isotopes from the Thamama-B reservoir and its surrounding dense zones are surprisingly limited, given the economic importance of these strata. Only three studies contain profiles of whole-rock (or micritic matrix) analyses covering the entire Thamama-B zone, all from Abu Dhabi onshore field F:

Oswald *et al*. (1995) presented profiles of whole-rock oxygen isotope analyses through the Thamama-B zone and the lower part of the DA in one crestal (oil-zone) well and one flank (water-zone) well from an onshore Abu Dhabi oilfield (field F according to the field outline and well locations in their Fig. 2). These data (Fig. 14A) show systematically more negative values (around -8.5‰) in the flank well B than in the crestal well A (around -8.0‰), which they interpret as resulting from greater amounts of calcite cement formed at high temperatures in the flank location after oil had arrived in the crestal area to inhibit] cementation.

Morad *et al*. (2016; 2019) showed profiles and cross-plots of C, O and Sr isotope analyses of small

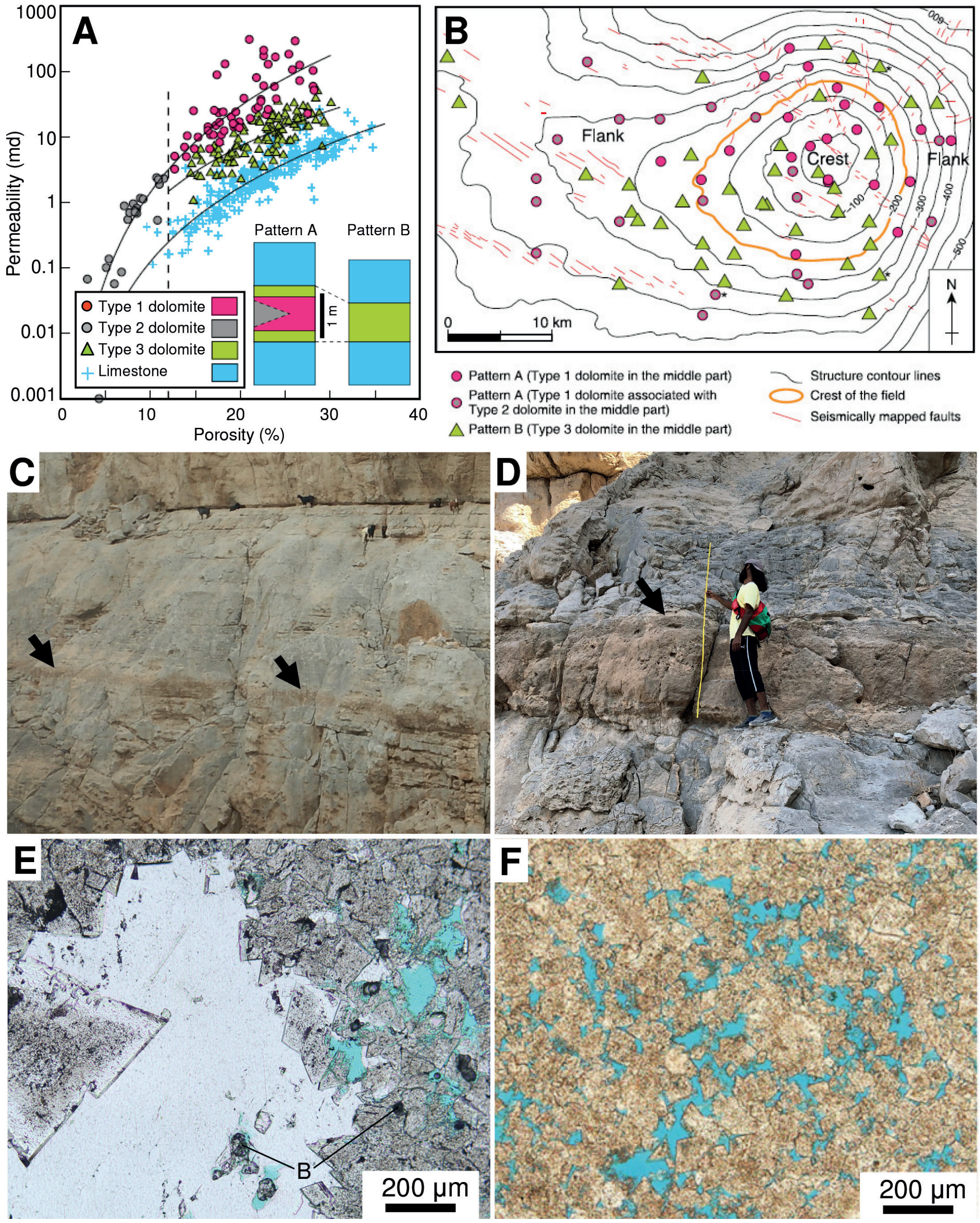

Fig. 12. Thamama-B dolostones. (A) RCA measurements in and around the dolostone layer in the lower part (sub-zone IV) of the Thamama-B zone in field J. Diagram illustrates patterns of occurrence of the three dolomite types defined by Yamamoto *et al.* (2018). Type 1 has well-developed intercrystalline pores. Type 2 has pores mostly occluded by dolomite cement, resulting in porosity <12% (dashed line). Type 3 has pores occluded by micritic calcite.
(B) Map showing distribution of dolomite patterns in field J.
(C) Dolostone layer (brown with arrows at top surface) in north wall of Wadi Rahabah (location in Fig. 3). Alteneiji *et al.* (2024) picked the DA/Thamama-B contact just above the dolostone, whereas previous workers picked this considerable higher in the section, approximately at the level of the goats (van Buchem *et al.*, 2002, their Fig. 10; Vaughan *et al.*, 2004, their Fig. 4).
(D) Closer view of dolostone layer in south wall of Wadi Rahabah (location shown in Fig. 3B of Alteneiji *et al.*, 2024). Yellow measuring stick (2 m) for scale.
(E) Photomicrograph of sample from near the centre of the Wadi Rahabah dolostone layer. Pores (blue-impregnated) are mainly formed by dissolution of dolomite and later coarsely crystalline calcite cement (white). Dark masses are bubbles in epoxy (B).
(F) Photomicrograph of Type 1 dolomite from the field J dolostone layer. A), B) and F) modified from Figs. 6, 3 and 5B, respectively, of Yamamoto *et al.* (2018).
Reprinted by permission of the AAPG whose permission is required for further use.

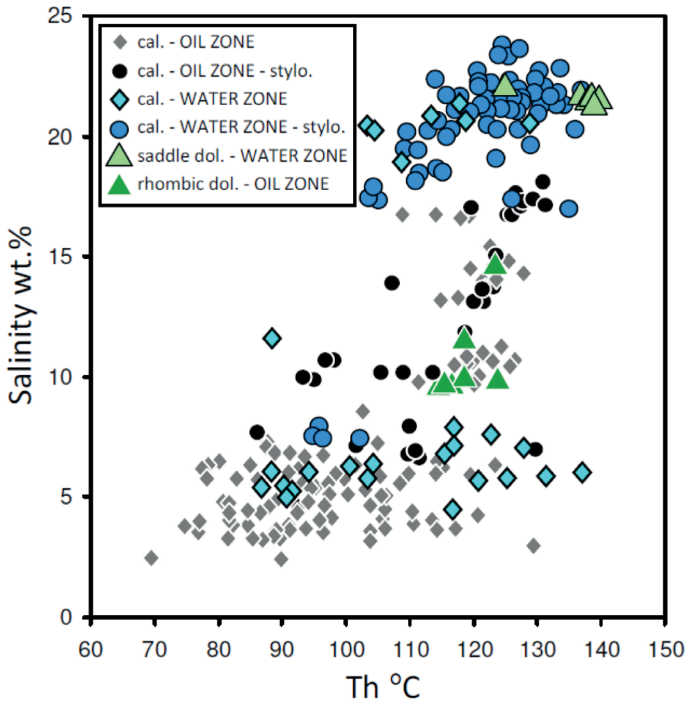

Fig. 13. Analyses of primary aqueous fluid inclusions from field F. Redrafted from Figure 13 of Morad *et al.* (2019). The temperatures for samples from crestal wells (oil zone) and flank wells (water zone) overlap, but the flank temperatures tend to be higher and with waters of higher salinity.

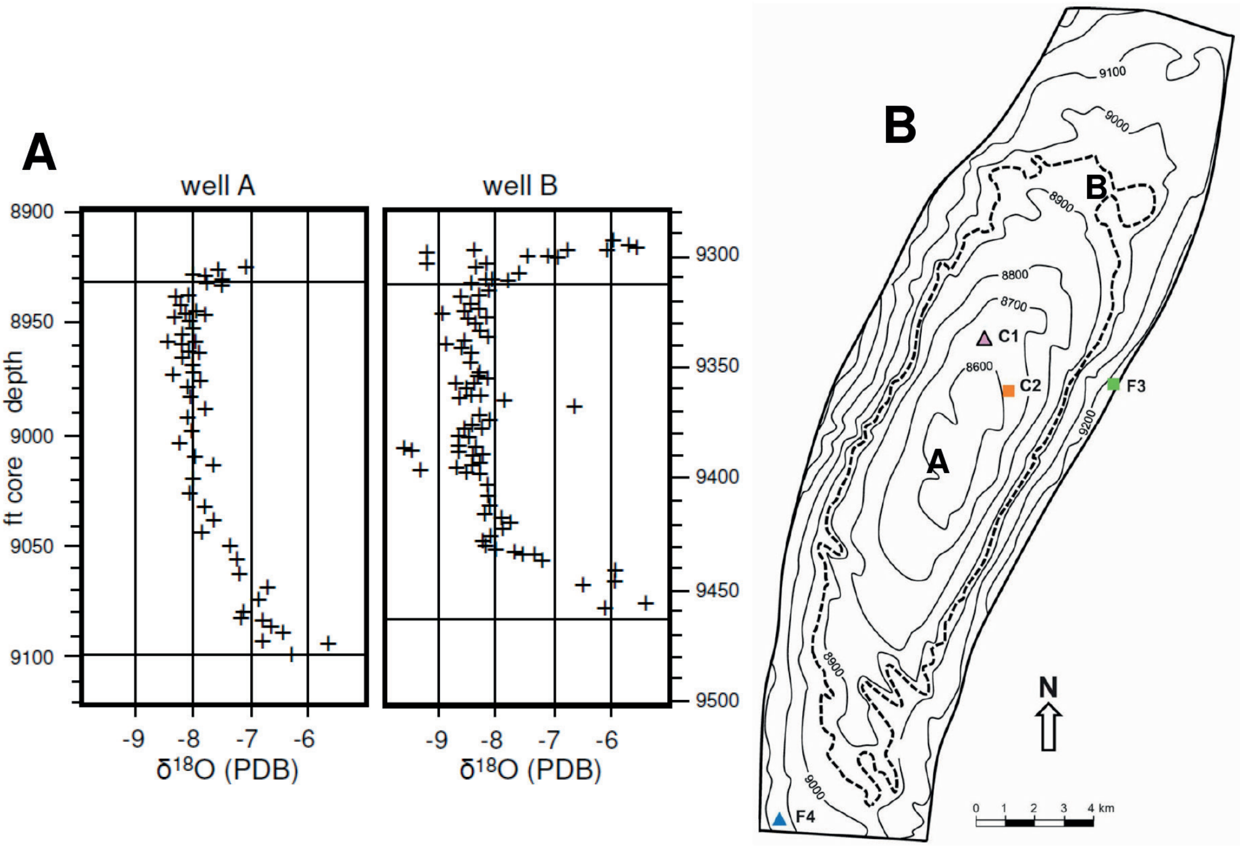

Fig. 14. (A) Oxygen isotope analyses from field F (depth scale in feet subsea). Drafted after Figure 6 of Oswald *et al.* (1995). Horizontal lines represent the top and base of the Thamama-B zone.
(B) Structural map of field F (top Thamama-B zone), showing locations of wells A and B of Oswald *et al.* (1995) and of wells studied by Ehrenberg *et al.* (2016; 2019) and Morad *et al.* (2016; 2019). Thin lines are 100-ft (30-m) contours below sea level. Dashed line is free-water level. Modified from Figure 3 of Ehrenberg *et al.* (2016).

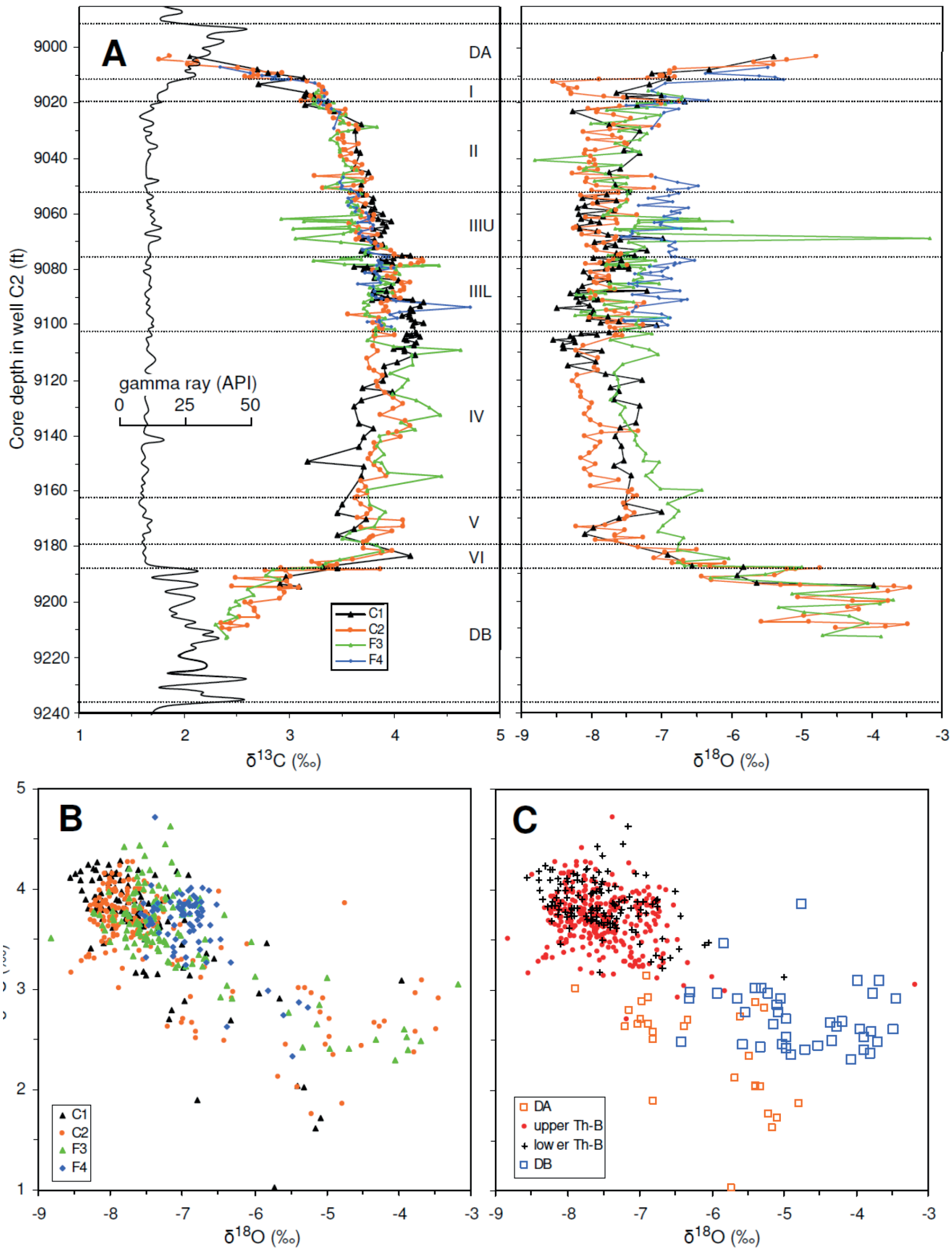

Fig. 15. Whole-rock C and O isotope analyses from field F. (A) Profiles with depths in wells C1, F3 and F4 adjusted to match depth intervals of each sub-zone in well C2. GR profile of well C1 (from Ehrenberg *et al.*, 2018) is also adjusted to match sub-zone depths in well C2.
(B) Cross-plot with symbols indicating wells.
(C) Cross-plot with symbols indicating stratigraphic intervals.

chips and micro-drilled samples of micritic matrix and cements from the Thamama-B zone in two crestal wells and two flank wells of an onshore Abu Dhabi oilfield (field F according to the map location and field outline in their Fig. 1). C versus O isotope cross-plots show extensive overlap between crestal and flank values for both calcite and dolomite, but the authors did not comment on the possible reasons for the similar average and range of O isotope values in crestal versus flank wells.

Ehrenberg *et al.* (2016) provided a data-repository file listing C and O isotope analyses of whole-rock core samples from the same four wells in field F as Morad *et al.* (2016), but using 100-300 g samples that were homogenized by grinding and also analyzed for bulk chemistry (Figs 15 and 16). Most samples correspond with a plug location having conventional-core-analyses of porosity, permeability and grain density. To facilitate comparison, the sample depths of wells C1, F3 and F4 in Fig. 15A have been adjusted to match the depth range of each reservoir zone in the crestal well C2. All four wells show similar overall trends of decreasing C and increasing O values both upwards and downwards from the main part of the Thamama-B reservoir into the

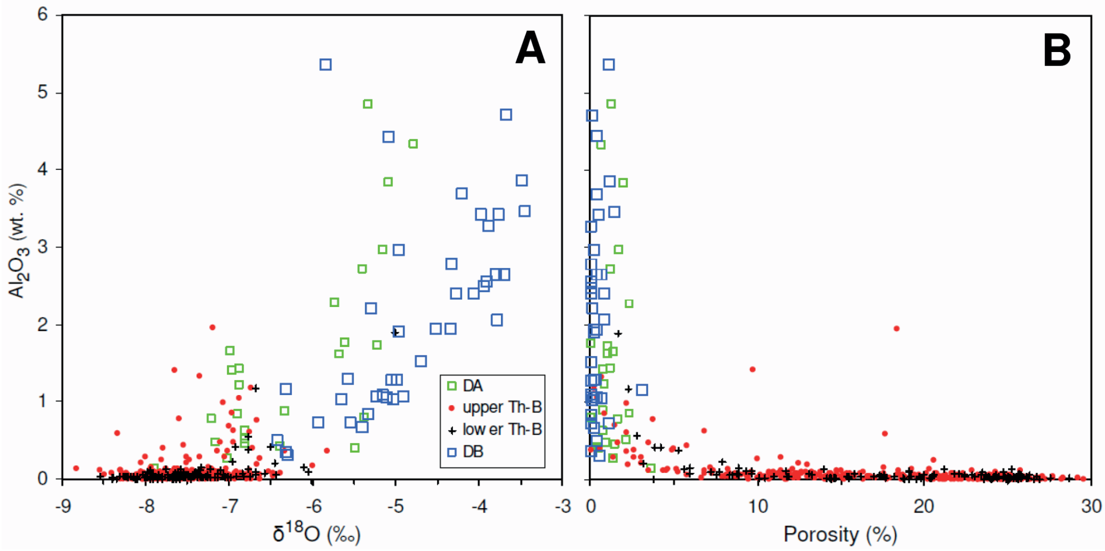

Fig. 16. Analyses from field F (Ehrenberg *et al.*, 2016; Ehrenberg and Wu, 2019). (A) Whole-rock alumina vs. oxygen isotope ratio. (B) Whole-rock alumina vs. routine-core-analysis porosity. Symbols indicate stratigraphic interval.

enclosing dense zones. There are, however, numerous local departures from the overall pattern, especially for the two flank wells in units IIIU and IIIL and for the oxygen isotope values of well C2 in unit I (Fig. 15A). Overall differences between wells and zones are also displayed in Figure 15B and C and by the average C and O isotope values listed in Table 1. Although a few obvious outliers (Fig. 15) should perhaps be excluded, these few extreme values have negligible effect on the averages.

Several other studies have presented selective analyses of either C isotopes alone or both C and O isotopes of selected samples or of intervals including only part of the Thamama-B zone:

1. Neilson *et al.* (1998) plotted C versus O isotope analyses of calcite cements and micritic grains from Thamama-B cores in as many as 20 wells in unidentified locations.

2. Cox *et al.* (2010) presented ion-microprobe analyses of C and O isotopes in bulk micrite and in zoned syntaxial calcite cements precipitated on echinoderm fragments in core samples from the oil zone and the water zone of the Thamama-B zone in an offshore Abu Dhabi field (probably field J). More negative O values in the micrites of the water zone (average of -7.4‰) than in the micrites of the oil zone (average of -6.2‰), together with lower porosity in the former, are interpreted as reflecting precipitation of further micrite cement at greater burial depths in the water zone. Outward-decreasing $\delta^{18}O$ values in the syntaxial overgrowths are interpreted as indicating increasing temperature as cementation progressed.

3. Vahrenkamp *et al.* (2010) displayed profiles of C isotope data from five wells at field B in Abu Dhabi, from six Oman fields, and in the Wadi Mu'aydin and Huqf High outcrop sections of Oman (as well as O isotope profiles in four of these wells), mainly for the Shuaiba Formation, but extending through the underlying DA and for several metres into the upper part of the Thamama-B zone.

4. Strohmenger *et al.* (2010) showed C isotope profiles through the uppermost 10-20 m of the Thamama-B zone, the DA and the overlying Shuaiba Formation in three wells from an onshore Abu Dhabi oilfield (field V according to the location map of their Fig. 1a).

5. Yamamoto *et al.* (2013) presented a profile of C and O isotope analyses in the uppermost 7 m of the Thamama-B zone, the DA and the overlying Shuaiba Formation in a core from an offshore Abu Dhabi oilfield (field W according to the location map of their Fig. 1a).

6. Vahrenkamp *et al.* (2014; their Fig. 7) and Barata *et al.* (2015; their Fig. 6) showed a plot of whole-rock C and O isotope data from the Thamama-B zone of several onshore Abu Dhabi fields as background for their clumped-isotope studies (*described below*).

7. Yamamoto *et al.* (2018) reported C and O isotope analyses of 16 dolostone and four limestone samples in a study of a thin (1.1 m) stratiform dolostone layer in an offshore Abu Dhabi field (field J according to their Fig. 3 map of field outline and depth contours). They also reported values of 5.30-5.89‰ SMOW for three samples of formation water from three widely spaced (16-27 km) locations on the field flanks (Fig. 17).

8. Steuber *et al.* (2022) showed profiles of C and O isotope ratios and bulk chemical analyses covering the upper 2.4 m of Thamama-B, the entire DA and the lower part of the overlying Shuaiba Formation in a core from around 2500 m below seafloor in an offshore Abu Dhabi well.

Several studies report whole-rock C and O isotope profiles from outcrop sections that include

Table 1. Average values of C and O isotope ratios measured in each well and zone of field F and temperatures calculated from different assumed values of water $\delta^{18}O$ SMOW using equation (1). Coloured cells indicate average water composition and temperature suggested for each stratigraphic interval.

Well	$\delta^{13}C$	$\delta^{18}O$	n	T°C for W $\delta^{18}O$=2‰	T°C for W $\delta^{18}O$=5‰	T°C for W $\delta^{18}O$=8‰
dense-A zone						
C1	2.2	-6.1	10	60	79	101
C2	2.5	-6.5	12	62	82	105
F4	2.7	-5.6	5	57	76	98
uppermost Thamama-B zone (sub-zone I)						
C1	3.9	-7.8	97	71	92	116
C2	3.3	-7.8	12	71	92	116
F3	3.3	-7.0	8	68	86	109
F4	3.3	-6.7	7	66	84	107
main Thamama-B zone (sub-zones II, IIIU, IIIL, IV, V)						
C1	3.8	-7.8	71	71	92	116
C2	3.8	-7.8	132	71	92	116
F3	3.7	-7.4	109	68	89	112
F4	3.8	-7.0	87	66	86	109
lowermost Thamama-B zone (sub-zone VI)						
C1	3.3	-6.6	1	63	83	105
C2	3.6	-6.7	8	64	84	107
F3	3.3	-6.1	4	60	80	102
dense-B zone						
C1	3.1	-5.3	4	55	74	96
C2	2.8	-4.8	24	51	70	91
F3	2.6	-4.7	13	51	70	90

strata correlative with the subsurface upper Kharaib Formation. These areas are nearer the open-ocean margin of the platform where the strata are thinner and include tidal-flat facies and numerous exposure surfaces not seen in the subsurface

Wagner (1990) presented profiles of C and O isotope analyses from three outcrop locations and five wells in northern Oman.

van Buchem *et al*. (2002; their Figs. 8 and 10) showed C isotope profiles from the Lekhwair-7 well (Oman) and Wadi Mu'aydin covering the Shuaiba Formation and the DA and extending 5-10 m into the upper part of the Thamama-B zone.

Sattler *et al*. (2005; their Fig. 5) showed C and O isotope profiles in the Huqf and Jabal Madar areas of eastern Oman.

Huck *et al*. (2017) analyzed C and O isotope profiles of bulk-carbonate and component cements, dolomite, bivalves and micrite from the Thamama-B-equivalent and surrounding formations at Jebel Madar.

Alteneiji *et al*. (2024) showed bulk-carbonate C and O isotope profiles for the Kharaib and Shuaiba formations in Wadi Rahabah.

Several of the above studies use the equations of Friedman and O'Neil (1977) or Kim and O'Neil (1997; the basis for equation 1 above) to calculate the O isotopic composition of waters from which calcite cements were precipitated (or, for dolomite, the equation of Land, 1983):

Neilson *et al*. (1998) used their fluid inclusion homogenization temperatures of calcite cements to calculate $\delta^{18}O$ ranges of 0-15‰ SMOW for the precipitating water, which they suggested may indicate a high degree of water-rock interaction at low water-rock ratios prior to calcite precipitation.

Cox *et al*. (2010) calculated water compositions of -6‰ to 5‰ SMOW (average 0‰) from early calcite cement $\delta^{18}O$ values of -7‰ to -1‰ using assumed temperatures of 20-50°C. For the latest cements, the average $\delta^{18}O$ of -9‰ (range of -10‰ to -7‰), assuming the current reservoir temperature of 100°C, gives water of 2‰ SMOW. They suggested these results were consistent with a trend towards increasing ^{18}O-enrichment of the formation waters with increasing temperature during burial.

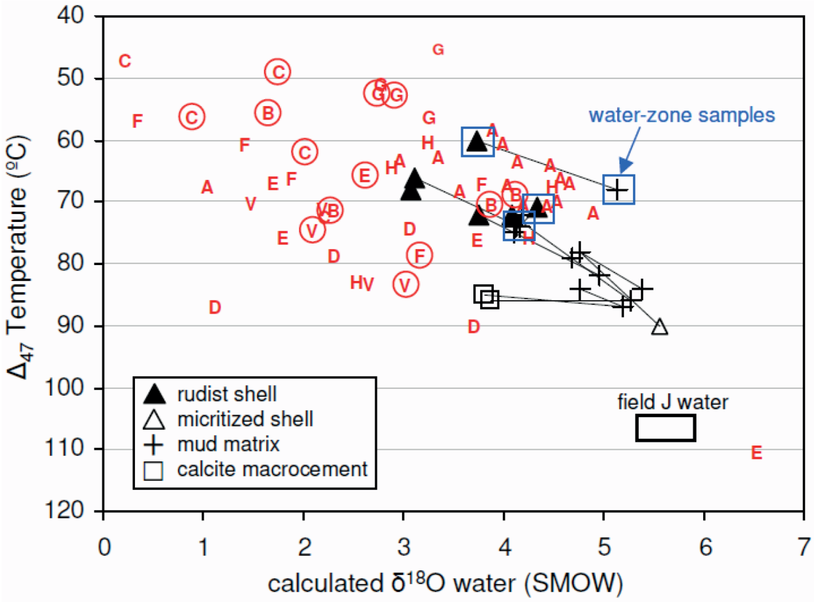

Fig. 17. Clumped-isotope analyses of Thamama-B and dense-A samples. Black symbols are data from Adlan and John (2023) with lines connecting analyses from same sample. Blue squares indicate two shell-matrix pairs from the water zone. Red symbols are bulk-rock analyses from fields identified by capital letters in Fig. 3 (data for field A from Vahrenkamp *et al.*, 2014; data for other fields from Barata *et al.*, 2015). The box at lower right shows the range of oxygen isotope values and flank reservoir temperatures for three water samples from the flanks of field J (Yamamoto *et al.*, 2018).

Morad *et al.* (2019) used their fluid inclusion Th values of blocky calcite cements to calculate water $\delta^{18}O$ of 0.3 to 10.2‰ SMOW. For replacive "rhombic" dolomite, Th = 115–124°C gave water $\delta^{18}O$ of 4 to 6‰ SMOW. For saddle dolomite cement, Th =122–140°C gave water $\delta^{18}O$ of 6 to 8‰ SMOW.

Clumped-isotope analyses of calcite samples can uniquely determine both the temperature of equilibration and the $\delta^{18}O$ of the water involved. Clumped-isotope studies of Thamama-B core samples have been reported in three publications: Vahrenkamp *et al.* (2014), Barata *et al.* (2015), and Adlan and John (2023) (Fig. 17):

1. Vahrenkamp *et al.* (2014) presented analyses of four to six samples in each of three wells in "field B" (field A, as shown in Fig. 3 of the present study, according to map location and field outline in Vahrenkamp *et al.*, 2014). Temperatures of 65-72°C for matrix recrystallization correspond to burial depths of 650-1100 m in Turonian to Campanian time (94-72 Ma). Precipitating waters have calculated $\delta^{18}O$ of 3.3-4.8‰ SMOW.

2. Barata *et al.* (2015) analyzed four to five whole-rock samples in one selected well from each of eight different oilfields (38 samples in total with calculated temperatures of 45-111°C and calculated water compositions of 0.2-6.5‰ SMOW). Petrographic observations of thin sections from the same samples were used to define cut-offs to eliminate samples having either >15% intraclasts or >15% cement in order to focus on the 13 samples from six fields containing dominantly mud matrix. These samples had a narrower range of calculated temperatures (49-84°C) and $\delta^{18}O$ of equilibrated water (0.9-4.1‰ SMOW). When combined with burial histories, these temperatures correspond to depths of 610-1370 m and ages of matrix recrystallization of Cenomanian to Campanian (101-72 Ma). Both Vahrenkamp *et al.* (2014) and Barata *et al.* (2015) interpret the results as supporting a model of micrite recrystallization in response to long-range water flow driven by ophiolite obduction hundreds of kilometres to the east. Subsequent modelling studies (Wei *et al.*, 2021), however, could not validate this model even though hydrodynamic conditions likely caused the movement of deep brines into the Thamama layers. However, chemical conditions assumed in the modelling study did not favour the required full-scale recrystallization of Thamama-B strata in the Abu Dhabi subsurface.

3. Adlan and John (2023) analyzed individual textural elements (rudist shell fragments, micritic matrix and coarse calcite cement) from ten samples in an onshore oilfield and one sample from an offshore field (Fig. 17). Previous studies had analyzed only bulk samples, potentially obscuring variations among different components. The calculated $\delta^{18}O$ of equilibrated waters range from 3.1-5.6‰ SMOW, similar to those of earlier studies (Vahrenkamp *et al.*, 2014; Barata *et al.*, 2015). However, they proposed closed-system water-rock interaction that primarily occurred within the matrix from the Late Cretaceous into the Paleocene, with matrix recrystallizing

continuously towards deeper burial and higher temperatures. The skeletal grains recrystallized earlier in an open water-rock system. Potential resetting of the clumped isotopes (Looser *et al*., 2023) was studied by Adlan *et al*. (2023) with results indicating that recrystallization during progressive burial, rather than solid-state reordering, appears to be responsible for the observed temperature records.

Formation waters

The present-day water column must be density-stratified, insofar as the shallow Abu Dhabi groundwater varies from fresh to brackish composition in inland areas near meteoric recharge to more saline nearer the Gulf coast (Murad *et al*., 2011; Zhang *et al*., 2017), and the biota of benthic foraminifera, algae and bivalves indicate that the entire Thamama-B and its surrounding dense zones were deposited in seawater of normal salinity. Formation waters in the oilfields, however, are highly saline: 17.2 weight % total dissolved solids in field A (Stenger *et al*., 2008), 18.2% in field B (Alsharhan, 1993b) and 19.1% in field F (Ehrenberg and Wu, 2019). More complete analyses of the chemical composition of the oilfield waters have not been published, but the high salinity is believed to result from the dissolution of deeper-lying Infracambrian salt, movement of which has formed large domal oilfield structures, diapirs and piercements in the area (Alsharhan *et al*., 2014).

Yamamoto *et al*. (2018) reported Sr-isotope analyses of Thamama-B formation waters from field J that are 0.00028 higher than Barremian seawater. Sr-isotope ratios reported by Neilson *et al*. (1998; their Fig. 9) for Kharaib Formation grains and cements are around 0.057 higher than Barremian seawater, reflecting interaction with radiogenic basement sources. Thamama-B cores from flank (water-zone) wells in field F have higher Zn contents (mostly 20-120 ppm) than cores from crestal (oil-zone) wells (mostly 0-30 ppm), which Ehrenberg *et al*. (2016; their Fig. 9C) interpreted as indicating late precipitation in flank locations of trace amounts of sphalerite from deep formation waters; precipitation was by contrast inhibited in the Thamama-B at the crest of the structure by the presence of oil.

DISCUSSION

Sedimentologic interpretations

Insofar as the Kharaib Formation was deposited on an epeiric platform having little or no seaward slope across hundreds of kilometres, it seems incorrect to apply the depositional model of a carbonate ramp, as suggested by Strohmenger *et al*. (2006), Ottinger *et al*. (2012), Tendil *et al*. (2022), Alteneiji *et al*. (2024) and Gatel *et al*. (2024), where fluctuations in water depth are expressed by lateral migration of shoreline-parallel facies belts. On an epeiric platform, metre-scale variations in depositional energy (recorded in terms of grain size and mud content) likely reflect both high-frequency cyclicity of water depth and storm events, with both types of causes tending to produce laterally extensive facies changes unrelated to landward-seaward orientation. Thus no one palaeogeographic diagram can suitably portray the overall spatial distribution of depositional environments; rather, a series of such diagrams is required, as exemplified by Figure 13 of van Buchem *et al*. (2002). Contrary to this view, Gatel *et al*. (2024; their Fig. 4a) presented a correlation model indicating progradation of lower Thamama-B strata from NW to SE across Abu Dhabi (from field K to field I, as identified in Fig. 3A). This model is inconsistent, however, with the layer-cake correlation of the lower Thamama-B reservoir sub-zones across the same fields (as well as field J; Fig. 5) and the lack of a palaeogeographic model that might account for this direction of progradation. Results from Dujoncquoy *et al*. (2018), van Buchem *et al*. (2002; Fig. 1) and Hillgartner *et al*. (2003), for example, show the platform as having evolved into an epeiric geometry, with its interior platform-lagoon (all of Abu Dhabi) undergoing aggradational, rather than large-scale progradational, accumulation from late Hauterivian time (lower Lekhwair Formation) until development of the intrashelf Bab Basin in the early Aptian. The steep seaward margin of the platform, however, prograded mainly toward the northeast throughout this time (Hillgartner *et al*., 2003).

Thamama-B stylolites and dissolution seams are an important aspect of the sedimentology because they are interpreted as having been localized by depositional clay, which was then further concentrated as insoluble residue as chemical compaction progressed (Ehrenberg *et al*., 2016). These features have a wide range of morphologies, including all the varieties described by Koehn *et al*. (2016). The fundamental role of electrically charged clay and mica surfaces in causing chemical compaction on all scales is well supported by observational evidence (Ehrenberg, 2022), experimental evidence (for quartz; Kristiansen *et al*, 2011), as well the theoretical application of the experimental results to carbonates (Walderhaug *et al*, 2006).

Sequence stratigraphic interpretations

The main sequence stratigraphic pattern in the Thamama section is the alternation of thick intervals of porous, clean limestone with thinner platform-wide zones of tight argillaceous limestone (likely having much greater pre-compaction thickness). The episodic influx of siliciclastic fines to form the dense zones is linked with falls in sea level, but Davies *et al*. (2002) listed three possible mechanisms that might account for episodic clay influx: supply from land areas, variations in climate, and volcanic ash falls. The latter mechanism seems implausible, however, because X-ray diffraction analyses show that the clay of the Thamama dense zones is mainly illite-smectite, mostly with only 15-25% expandable layers, plus subordinate dickite (Ehrenberg and Wu, 2019), thus lacking any discrete smectite component indicative of a volcanic ash. The following three hypotheses may thus be proposed:

1. Falls in relative sea level could result in an increased supply of clay due either to hinterland uplift or increasing stream gradients and land areas. Alternating argillaceous and clean carbonate hemi-cycles that infilled the Bab Basin during Upper Shuaiba deposition are attributed to the former mechanism (Maurer *et al*., 2010). X-ray diffraction analyses of Upper Shuaiba argillaceous zones (Al Habsi *et al*., 2014) reveal clays of similar types and proportions as in the Thamama dense zones (Ehrenberg and Wu, 2019).

2. Climatic variations can be linked with eustacy (Soreghan, 1997), with clay influx caused either by increased humidity during falls in sea level (Pittet *et al*., 2002; van Buchem *et al*., 2002) or by increased aridity and wind-blown dust during sea level falls (Ehrenberg and Wu, 2019).

3. Siliciclastics were concentrated by much slower accumulation of carbonate sediment, possibly aided by siliciclastic influx by either of the above mechanisms or simply by stagnation of water circulation following the fall in sea level.

In any case, the siliciclastic-rich dense zones seem best interpreted as early transgressive deposits based on the principle of reciprocal carbonate/siliciclastic sedimentation (Wilson, 1967; 1975) and by analogy with the pattern of cyclic siliciclastic-rich and siliciclastic-poor sedimentation in the Upper Shuaiba clinoforms infilling the Bab Basin (Maurer *et al*., 2010; Al Habsi *et al*., 2014).

Preservation of porosity by oil

The Thamama-B porosity-depth trend is even more favorable if only oil-zone data are considered (heavy black symbols in Fig. 6), and it has long been surmised that early oil emplacement has preserved porosity in the crests of Thamama-B fields (Oswald *et al*., 1995; Neilson *et al*., 1996; 1998; Kirkham *et al*., 1996). As shown by the dotted red lines in Fig. 6, depth trends within individual fields are much steeper (17% /1000 ft; 5.2%/100 m) than the overall trend (around 2.5%/1000 ft; 0.75%/100 m). The gradual decrease in porosity downward through the oil zone in each of fields A and F of Fig. 6 (also observed in fields C and J; Fig. 9A of Ehrenberg *et al*., 2020a) may result from the thick transition zones of these fields, reflecting the dominance of microporosity (Kirkham *et al*., 1996; Perrin *et al*., 2020), but could also result from gradual filling of the structures as cementation progressed. Zone thickness also decreases down-flank because of increasing chemical compaction along stylolites (Melville *et al*., 2004; their Figs. 3 and 4; Ehrenberg *et al*., 2020a; their Figs 9A and 18A). However, the Thamama-B reservoir in several other fields does not display upward-increasing porosity towards the crest, possibly for reasons outlined by Ehrenberg *et al*. (2020a) in connection with their Figure 9B, including shallow burial depth (1092–1808 m = 3584–5932 ft) in four cases, little crest-flank depth difference in three other cases, extensive reservoir compartmentalization in the case of field N, and massive leakage and partial loss of the oil column in the case of field B.

As summarized above, the range of proposed times for migration of oil into Thamama-B fields is 80-20 Ma (Gumati, 1993; Taher, 1997; 2019). An Oligocene/Miocene timing seems to be the more current view, however (Taher, 2019), and this is consistent with the temperature of 110ºC derived from the different maximal crest and flank fluid inclusion temperatures (Figs 13, 18).

Lambert *et al*. (2006) proposed that the trends of increasing porosity towards the tops of unspecified domal Middle East oilfields (but not necessarily the Thamama-B fields illustrated in Fig. 6) at least partly result from burial dissolution by acidic waters attending, or shortly preceding, emplacement of oil. However, theoretical problems with this mechanism were noted by Ehrenberg *et al*. (2012), and the hypothesis of porosity enhancement by late dissolution is essentially disproven by the observation that solidity (formation thickness with porosity removed) is in general invariant between crests and flanks in several of the largest structures having crestal porosity increase (Ehrenberg *et al*., 2020a; Fig. 3B).

Preservation of limestone porosity by liquid petroleum is also observed in other Cretaceous and Jurassic oil reservoirs (Brasher and Vagle, 1996; Heasley *et al*., 2000; Al-Ansi *et al*., 2012; Hollis *et al*., 2017; Alsuwaidi *et al*., 2022; Cross *et al*., 2022; Ehrenberg *et al*., *in prep.*) and in one gas-condensate field (Van Simaeys *et al*., 2017), but is not known or doubtful in other carbonate reservoirs (Neilson *et al*., 1998) and in sandstone reservoirs (as reviewed by Taylor *et al*., 2010). Reservoir rocks in most of the above cases are highly microporous, so it can be suspected that a preponderance of microporosity in limestone reservoirs may be favorable for the preservation of porosity by oil. This could be the case if micropore surfaces are somehow more susceptible to oil wetting than macropore surfaces, thus reducing both the surface area available for cement precipitation and the cross-sectional area of the path of aqueous diffusion through which the cementing ions must travel from their origin along stylolite surfaces to the sites of precipitation in the pore system. Bjørkum *et al*. (1998) showed how porosity preservation by oil is theoretically proportional to the length of this path during quartz cementation in sandstones, and similar constraints should apply regarding the effect of reducing the cross-sectional area of the path.

Although the solidity data indicate little or no mesogenetic porosity creation in the crestal regions of Thamama-B fields, it remains to be determined whether crestal porosity was enhanced by burial dissolution in the other cases noted above, as is suggested for Mauddud reservoirs in northern Kuwait by Ehrenberg *et al*. (*in prep.*). This possibility can be examined by comparison of solidity-thickness values derived from wireline logs to investigate whether crestal values are similar to flank values, as in Abu Dhabi, or systematically less, which could indicate removal of material by late dissolution.

Processes controlling formation water composition

Various models may be imagined for the origin of hypersaline formation waters at Abu Dhabi oilfields and how these have interacted with the Thamama-B reservoirs during their burial history.

The simplest scenario is that the present-day formation water is the product of mixing as strata subsided into a static water column, such that it was fundamentally the strata, rather than the water, undergoing the main component of movement, a model advanced earlier by Giles (1997, p. 371-372). If undisturbed by tectonics, a salinity-stratified water column, such as those documented in other basins (Hanor and Sassen, 1990; Gran *et al*., 1992; Heydari, 1997; Kharaka and Hanor, 2004), should be relatively stable over geologic time and would not be subject to mixing by thermal convection (Bjørlykke *et al*., 1988). Movement of the water into and through the strata during gradual subsidence would be focused along pathways of greatest permeability and connectivity, such as faults and the tensile fractures commonly present along stylolites. Impermeable layers, such as dense zones, would tend to retain the water and the mineral compositions acquired early in the burial history.

Alternatively, high-temperature "evolved" waters from greater depths may have moved upwards along fractures and entered the strata along permeable pathways. This process would be aided by overpressuring of the deeper strata, but all major Abu Dhabi fields have near-hydrostatic fluid pressure (Ehrenberg *et al*., 2020a; Nadeau *et al*., 2023). This is very different from the highly overpressured conditions associated with the formation of cemented fractures in equivalent strata in the Oman Mountains, some 200-400 km to the east of the Abu Dhabi oilfields (Gomez-Rivas *et al*., 2014).

A more elaborate proposal is long-distance lateral movement of water driven by compaction in the area of the Hajar Mountains caused by obduction of the Oman ophiolites (Vahrenkamp *et al*., 2015; Barata *et al*., 2015). Modelling by Wei *et al*. (2021) supports the overall viability of large-scale lateral movement of subsurface water as a result of ophiolite emplacement and compaction during the Late Cretaceous.

The fluid-inclusion results from field F (Fig. 13) indicate that major burial cementation began at around 75-80ºC, corresponding to around 1.5 km (5000 ft) burial depth, based on the present-day Abu Dhabi geotherm (Ehrenberg *et al*., 2020a; their Fig. 5). At this time, the formation water may have had a range of salinity similar to that of the fluid inclusions (3.5-7.5%; Fig. 13). The clumped-isotope data, however, indicate water compositions of 2-5‰ SMOW at 75-80ºC (Fig. 17), suggesting salinities much greater than seawater. But the clumped-isotope values are for bulk-matrix analyses (about one gram prepared with minimal content of cements and larger bioclasts), whereas the fluid inclusion data are point analyses from macrocements. It should also be kept in mind that calcite is a fairly soft mineral in which inclusions may be subject to stretching that could result in temperatures and salinities different from those at time of trapping (Goldstein and Reynolds, 1994).

Nevertheless, as burial continued, the formation water became more saline, with the fluid inclusions recording progressively wider ranges of salinity at each temperature increment. Finally, at the present-day reservoir temperature of 126ºC, the water attained a range of 6-24% salinity in flank locations and a somewhat lower range in the oil zone. Here again, it is always possible that the range of fluid inclusion values is greater than that of the waters originally trapped.

The overall higher salinities and homogenization temperatures of fluid inclusions "along stylolites" (Fig. 13) are consistent with the explanation by Morad *et al*. (2019) that basinal brines entered the Thamama-B limestones along stylolites. It is not necessarily the case, however, that these brines were derived from significantly greater depths than the current burial depth of the Thamama-B. Insofar as the present-day water of field F is "basinal", it is equally plausible that the water entering the limestone along stylolites and then mixing with the water already present in the pore spaces (derived from shallower depths) was simply the water that was already present at 2.7 km (roughly 9000 ft) depth, which remained in place as part of a static salinity-stratified water column through which the strata gradually subsided.

It is also questionable whether the presence of cements along stylolites necessarily indicates that water flow took place along the clay-lined stylolite surfaces. Bedding-plane stylolites are commonly viewed as conduits for water flow when they show evidence either of having opened to allow cements to accumulate or of dissolution having occurred along the stylolite surfaces (Braithwaite, 1989; Bruna *et al*., 2019; Gomez-Rivas *et al*., 2022; Pontes *et al*., 2023), especially when fluid pressures facilitate opening by exceeding overburden stress (Martin-Martin *et al*., 2018) or during uplift. Stylolites in Thamama-B reservoirs, however, generally show no signs of present or past (cement-filled) bedding-parallel openings, and all reservoirs have near hydrostatic fluid pressure. A study by Heap *et al*. (2014) suggested that stylolites may have had little overall effect on permeability because they tend to form discontinuous "perforated" layers with gaps through which fluids can move.

More plausible avenues for water ingress are the abundant tensile fractures that are commonly oriented roughly perpendicular to the stylolites and which thin and terminate within millimetres to centimetres of the stylolite surface. Water flow along these extensional features is suggested by the common presence of calcite, dolomite and dickite cements which fill them. These ubiquitous tensile fractures can presumably account for the observation that the stylolite-rich zones separating Thamama-B subzones in field J do not greatly affect vertical permeability, whereas the intense cementation associated with these stylolites nevertheless causes capillary pressure barriers that restrict slumping of injected seawater (Al-Ansari *et al*., 2000). Entry of water is also likely to have occurred using the abundant fractures associated with Late Cretaceous strike-slip faulting (Melville *et al*., 2004; Clarke *et al*., 2010).

Interpretation of carbon and oxygen isotope values

Following the example of Vahrenkamp (1996; 2010) for the Aptian Shuaiba Formation in Arabia, the carbon isotope values in Fig. 15 are interpreted as recording trends in secular seawater composition throughout the time of deposition. The trend of decreasing $\delta^{13}C$ values upwards into the DA (Fig. 15A) matches the lower part of a major excursion of Barremian-Aptian seawater composition documented in carbonate sections throughout Asia and Europe (Van Breugel *et al*., 2007; Vahrenkamp, 2010). The trend of decreasing $\delta^{13}C$ downwards into the DB (Fig. 15A) is similarly consistent with the shift in global carbonate $\delta^{13}C$ toward more positive values from early Barremian to mid-Barremian time reported by Weissert *et al*. (1998; their Fig. 2) and Weissert and Erba (2004; their Fig. 2).

By contrast, the oxygen isotope trends in Fig. 15 are interpreted as a result of variations in both water composition and temperature during the burial history of field F. The stratigraphic trends toward less negative $\delta^{18}O$ approaching both the upper and lower contacts of the Thamama-B zone (Fig. 15A) can be explained as reflecting earlier cementation in the dense zones than in the main, central part of the porous reservoir section, with the top and basal Thamama-B sub-zones I and VI having intermediate degrees of timing and cementation intensity. Following near-total porosity loss at shallow depths (well before oil arrival), the dense zones would have become closed to rock-water isotopic exchange (Czerniakowski *et al*., 1984), preserving the oxygen isotopic signature of water nearer to seawater composition than the present-day formation water as temperatures increased from around 30ºC to perhaps as high as 70ºC. The porous reservoir would have continued isotopic exchange in a more open system as burial progressed, thus acquiring more negative oxygen isotopic compositions.

Although the actual salinity gradient of the Abu Dhabi formation water column is not known, it is evident that the oilfield waters are highly saline and have high $\delta^{18}O$ (based on the clumped-isotope data and the water analyses from field J; Fig. 17). Shallower waters are inferred to be less saline, based on the assumption that the low-salinity fluid inclusions (Fig. 13) represent trapping of shallow waters in earlier cements. In any case, the earliest cementation must have involved waters with salinity nearer to seawater and low $\delta^{18}O$ (nearer the range of 0-1‰ SMOW of global benthic foraminiferal oxygen isotope data for Barremian/Aptian time; O'Brien *et al*., 2017).

Within the above context, it is proposed that cementation took place in stages with progressively more saline and isotopically more positive waters as the Thamama section was gradually buried to higher temperatures. The dense zones would have been completely cemented in waters having $\delta^{18}O$ somewhat more positive than seawater (perhaps around 2‰ SMOW; Table 1, although cementation and re-equilibration of matrix and bioclasts probably took place over a range of time, as temperatures and water $\delta^{18}O$ gradually increased). Near the top and basal Thamama-B contacts, frequent laminations of depositional clay promoted early stylolite development and associated cementation, with these cements forming from waters having a relatively higher oxygen isotope composition (perhaps around 5‰ SMOW; Table 1). In the main part of the Thamama-B zone, moderate clay abundance would have resulted in slower cementation, as temperature, salinity and water $\delta^{18}O$ gradually increased. This process was slowed by the arrival of oil in the crestal wells, but continued with higher temperatures and more positive water $\delta^{18}O$ in the flank wells (with the average water composition hypothetically reaching around 8‰ SMOW; Table 1).

Regarding oil-zone (crestal) versus water-zone (flank) comparison of oxygen isotope data, the newer results for field F (Fig. 15 and similar profiles in

Morad *et al*., 2016; 2019) show the flank wells as having overall less negative $\delta^{18}O$ than crestal wells (Fig. 15B). This is the opposite of what Oswald *et al*. (1995) reported when comparing the crestal Well A versus the flank Well B in field F (Fig. 14). The reasons for this inconsistency are not known, but Oswald *et al*. (1995) gave no information about the samples and methods used. The newer results, however, raise the question of why flank oxygen-isotope values for the Thamama-B limestones would be similar to, or higher than, crestal values if the limestones in flank locations contain as much as 10 volume % more late calcite cement, presumably formed at higher temperature, than the cements in limestones in the crest. As shown in Table 1, the answer could be that the late cement in the Thamama-B in the flank wells was precipitated from deeper, higher-temperature waters having a positive oxygen isotope composition relative to the earlier-formed cements in limestones in the crestal wells. According to equation (1), waters of sufficiently higher average $\delta^{18}O$ could precipitate cements of higher $\delta^{18}O$ despite higher temperatures.

The results of Adlan and John (2023) show that the calcite composing Thamama-B limestone is heterogeneous in $\delta^{18}O$, with both matrix values and rudist shell fragments having re-equilibrated at various times during burial with waters having $\delta^{18}O$ much higher than that of Lower Cretaceous sea water. Analyses of coexisting shell and matrix from the same samples lie along a trend that can be interpreted as resulting from partial re-equilibration of each component and continued cementation as waters became heavier with higher temperatures during progressive burial (Fig. 17). Shells were less reactive due to coarser crystal sizes and thus lagged behind the more finely crystalline matrix. All of the Adlan and John (2023) samples were collected either from the lower 4 m of the DA or the upper 0-6 m of the Thamama-B zone. These locations all have low porosity and, according to Ehrenberg *et al*. (2016) and Ehrenberg and Wu (2019), were tightly calcite-cemented well before the arrival of oil due to abundant depositional clay that facilitated chemical compaction. Further re-equilibration with increasing burial may thus have been prevented by filling of most pore spaces by calcite cement. This hypothesis is supported by the similarity in isotope composition between analyses of limestone samples from the water zone (flank locations) and the oil zone (crestal location) of the onshore field (Fig 17).

Based on the results of Adlan and John (2023; Fig. 17), it can be estimated that average matrix material in the lowermost DA and uppermost Thamama-B zone equilibrated with waters having $\delta^{18}O$ of around 5‰ SMOW at 80-90ºC. Using equation (2), it can be seen that the range in calcite $\delta^{18}O$ corresponding with these values is -6.2 to -7.5‰, which overlaps with the range of average bulk-rock $\delta^{18}O$ values in the DA and the uppermost Thamama-B sub-zone (Table 1).

Timing of cementation

Morad *et al*. (2019) suggested that the fluid inclusion data of Fig. 13 reveal two cementation phases for Thamama-B limestones: one at 75–85°C before Late Cretaceous ophiolite obduction, and one at 85–125°C after ophiolite obduction. The time of obduction is suggested to correspond to a burial depth for the limestones of around 3.1 km. However, obduction in the Oman Mountains (Hawasina Complex) took place between 92 and 80 Ma (Scharf *et al*., 2021), whereas obduction of the Masirah ophiolite occurred at around 65 Ma (Schreurs and Immenhauser, 1999). Along the burial history of the Thamama-B in field F (Fig. 18), 92-80 Ma corresponds to depths of around 1.0-1.2 km (3281-3937 ft) and temperatures of 70-75°C. This is approximately the temperature at which burial cementation of the Thamama-B in field F began according to the fluid inclusion data (Fig. 13). Thus, it would seem that ophiolite obduction roughly coincides with, rather than pre-dates, the start of burial cementation, which supports the hydrodynamic model of compaction as a result of ophiolite emplacement and resulting westward water circulation proposed by Wei *et al*. (2021). Whether there was any significant effect of obduction on cementation is not known, but massive lateral flow of formation water as the result of tectonism is highly plausible (Heydari, 1997).

The model of Oswald *et al*. (1995; their Fig. 9) showed porosity preservation in the crest of field F (relative to the greater stylolitization and cementation of the flanks) as having occurred before regional southward tilting had raised the stylolite zone in the northern part of the field above the oil/water contact (OWC). Melville *et al*. (2004; their Figs. 20, 21, 26) showed seismic images indicating greater porosity and thickness of the Thamama-B zone offset to the north of the crest of field A, reflecting northward tilting subsequent to the main interval of porosity preservation due to the presence of oil. Kirkham *et al*. (1996) described post-late Miocene northeastward tilting of the Thamama-B reservoir in an offshore Abu Dhabi oilfield that resulted in relatively low porosity above the free-water level in the SW part of the field. Heydari-Farsani *et al*. (2020) showed that northward tilting by 0.84º in Miocene time may have been responsible for residual oil below the free-water level in oilfields in the Iranian sector of the Persian/Arabian Gulf.

The following model for cementation timing is proposed here for field F (Fig. 18) and may also be representative of the Thamama-B and enclosing dense zones in other Abu Dhabi fields:

Eogenetic cementation throughout the Thamama-B and its surrounding dense zones at and just below the

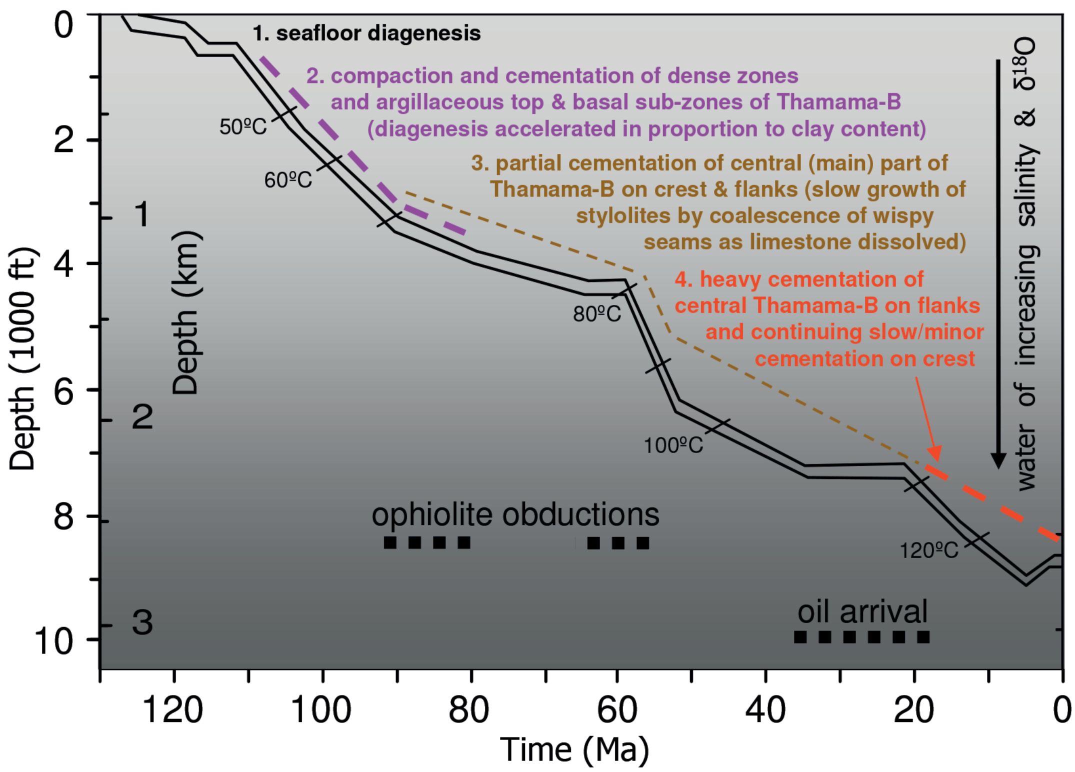

Fig. 18. Burial and thermal history of the top and base of the Thamama-B zone in field F (from Barata *et al.*, 2015) with the timing of diagenetic stages indicated by the dashed lines. Proposed times of oil arrival vary from Campanian to Late Cenozoic (Gumati, 1993; Taher, 1997; 2019), but the latter (shown here as late Oligocene to early Miocene) is preferred based on fluid inclusion data. Downward-darkening shading represents suggested salinity-stratification of the water column, but it is unknown to what degree this is gradual or abrupt.

sea floor was driven largely by calcium-carbonate stabilization and included: (i) finely crystalline pore-coating calcite that coarsens outward into minor equant spar; (ii) the earliest zones of syntaxial cement on echinoderm fragments; and (iii) microcement formed by micrite neomorphism. Incipient hardground cementation is observed at cycle tops within the DA (Ehrenberg and Wu, 2019) and is evidenced in the Thamama-B by common intraclasts of pebble to cobble size, in some cases forming distinctive rudstone beds (Ehrenberg *et al.*, 2018). Common *Glossifungites* horizons in upper Thamama-B also indicate episodic firmground development.

Cementation of the dense zones and the top and basal intervals of the Thamama-B (within 4-5 m of bounding upper and lower contacts), involving both macrocement completely filling larger pores and microcementation of mud matrix and intragranular micropores, began at low burial temperatures (40-60°C; with rate proportional to clay abundance), but accelerating to fill nearly all pore space before 80°C (purple cells in Table 1). Clumped-isotope data, however, show that the top Thamama-B interval and the lower part of the DA continued to be cemented and re-equilibrate as temperatures increased further (Fig. 17). Cementation of the calcite microcrystals composing mud matrix and microporous grains likely resulted in micro-zoned mixtures of primary marine and burial calcite (Hasiuk *et al.*, 2016).

Cementation of the main part of the Thamama-B zone in both crestal and flank locations was a gradual process that continued from about 75°C onward, but was greatly slowed in the crests by the arrival of migrating oil. Assuming a water composition of $\delta^{18}O$ = 5‰ SMOW and the average $\delta^{18}O$ values for the uppermost Thamama-B sub-zone in both crestal and flank wells and the main part of the Thamama-B in the crestal wells gives temperatures of 84-92°C (brown cells in Table 1).

Flank cementation continued and accelerated with increasing temperatures. The fluid inclusion data do not reveal any definite difference in homogenization temperatures between cores from crestal and flank wells that might be used to pinpoint a particular time on the burial curve, despite the flank inclusions being distinctly more saline and having somewhat higher homogenization temperatures overall than the crestal inclusions (Fig. 13). Nevertheless, a majority of water-zone temperatures are in the range 75-110°C, whereas the majority of oil-zone temperatures are 110-135°C, which may indicate an approximate average temperature of oil accumulation. Assuming a water composition of $\delta^{18}O$ = 8‰ SMOW and the average $\delta^{18}O$ values for the main part of Thamama-B in the flank wells gives temperatures of 109-112°C (red cells in Table 1).

The vertical distribution of porosity, stylolites and clay in the field F cores indicates control of calcite cementation and porosity loss by short-range diffusion and local precipitation of calcite dissolved by stylolitic compaction. Stylolites were localized by occurrences of clay that were concentrated at particular horizons and surfaces by primary depositional processes (Ehrenberg *et al*., 2016). Stylolite growth and associated cementation probably accelerated with increasing temperature, but rates also appear to have been proportional to clay abundance because clay-rich beds near the top and basal contacts of the Thamama-B zone underwent extensive chemical compaction well before oil emplacement, resulting in similar porosity loss in these intervals in both crestal and flank wells (Ehrenberg *et al*., 2016). The more intensely argillaceous DA and DB also underwent nearly total porosity loss before the arrival of migrating oil, as indicated by similarly low porosity and uniform thickness in both crest and flanks of field F (Ehrenberg and Wu, 2019).

In the main part of the Thamama-B zone, more dispersed local concentrations of clay developed into clusters of anastomosing wispy dissolution seams that subsequently coalesced in flank areas into high-amplitude stylolites. In crestal locations, however, the emplacement of oil arrested the process whereby wispy seams evolved into stylolites. The wide ranges of porosity and permeability in each well result mainly from stratigraphic variations in depositional clay that in turn have caused differences in stylolite development and thus local differences in calcite cementation.

A local, closed-system relationship between stylolite development and nearby precipitation of the dissolved carbonate is supported by overall correlation between porosity and both stylolite amplitudes and distance to the nearest stylolite in field F (Ehrenberg *et al*., 2016; their Figs. 10 and 11, respectively). Additional support is provided by the observation that, although chemical compaction in flank locations may reduce Thamama-B thickness by up to 22% (Melville *et al*., 2004), solidity remains constant (Ehrenberg *et al*., 2020a; their Table 2). This contrast is also apparent from a comparison of Fig 3A (which shows local thicks over fields A, C, F and J) with Fig. 3B (which shows no variations in solidity across these same fields).

CONCLUSIONS

1. Because Thamama-B and enclosing strata were deposited on an epeiric platform having little or no seaward slope across hundreds of kilometers, it is not appropriate to apply the depositional model of a carbonate ramp, where fluctuations in water depth would be expressed by lateral migration of shoreline-parallel facies belts.

2. Intervals richer in depositional clay are suggested to form in response to both major and minor falls in sea level and are thus fundamental to the recognition of 3rd-order sequences and component 4th-order cycles. Possible mechanisms causing clay enrichment during falls include (i) increased emergence of distant land areas, (ii) climate change, involving either increased aridity and related dust delivery or increased humidity and related run-off from exposed areas, and (iii) decreased carbonate production due to stagnation of the platform lagoon.

3. Numerous studies have concluded that higher Thamama-B porosity on the crests of domal fields results from inhibition of calcite cementation by oil. The strata are thinner on flanks because of stylolitic dissolution, but constant solidity (zone thickness with porosity removed) between crests and flanks indicates that burial dissolution did not contribute to the higher crestal porosities.

4. The profile of decreasing carbon isotope values from the Thamama-B zone both upwards and downwards into its surrounding dense zones likely reflects changes in global seawater composition. However, the profile of increasing oxygen isotope values from the Thamama-B zone into its surrounding dense zones appears best explained by precipitation of calcite cements and re-equilibration of matrix calcite at different burial depths and temperatures in waters that became progressively heavier in $\delta^{18}O$ with increasing depth.

5. A compilation of clumped isotope analyses of samples consisting mainly of micritic limestone matrix material shows overall correlation between $\delta^{18}O$ of water and temperature, which is similar in slope to the trend of coexisting rudist shells and their enclosing matrix. This correlation is consistent with varying degrees of re-equilibration and cementation of the limestones during progressive gradual burial in a salinity-stratified water column having heavier $\delta^{18}O$ at greater depth.

6. Fluid inclusion data indicate that major burial cementation began in the Thamama-B reservoir of field F at around 75-80 ºC, corresponding to around 1.5 km depth, and involved water near seawater salinity (3.5%) to somewhat higher (7.5%). Cementation continued up to the present reservoir temperature of 126 ºC, with water of widely varying salinity (up to 20-24%). Higher salinities in fluid inclusions along stylolites indicates that either these dissolution surfaces or their associated tensile fractures were preferred paths for influx of saline water from which late cements precipitated.

7. A 4-stage model for timing of calcite cementation and resulting porosity loss is proposed, involving: (i) eogenetic cementation at and just below the

seafloor, (ii) mechanical and chemical compaction and cementation of the dense zones and the argillaceous top and basal intervals of the Thamama-B zone beginning at 30-40°C and accelerating to fill nearly all pore space by 80-90°C, (iii) partly synchronous with stage 2, partial cementation of the main part of the Thamama-B zone starting at about 75°C, and (iv) acceleration of cementation in the water zone with increasing temperature after the arrival of migrating oil, probably around 110ºC, began to slow cementation in the crest. This late cementation involved waters of progressively increasing salinity and oxygen isotopic composition.

Points 4, 6 and 7 apply specifically to the relatively deeply buried field F, where the most comprehensive petrologic studies have been carried out, but are suggested to be relevant to Thamama-B reservoirs in other fields as well. The simplest model for Thamama-B diagenesis is that the main processes took place under relatively closed-system conditions (Bjørlykke and Jahren, 2012) as the strata subsided through a salinity-stratified water column. Nevertheless, addition of late calcite and exotic cements by influx of waters moving upwards along faults and fractures from deeper sources is also possible. A broader implication of the present study is that burial diagenesis of carbonate reservoirs can occur with little or no addition or removal of mineral mass as different reservoir regions become successively closed to further mineral-water interaction by expulsion of the water, either by cementation (as in the dense zones) or by arrival of oil (as in the structural crest).

ACKNOWLEDGEMENTS

Laura Galluccio initiated this review by inviting SNE to present the topic at an AAPG regional conference in Naples, June 2022. The paper was greatly improved by suggestions from Shawn M. Fullmer, Neil F. Hurley, James Bishop and an anonymous reviewer.

Data availability statement

The data used in this paper are all available from the previous literature sources cited here.

REFERENCES

Abou Zeid, Z.S. and El Bishlawy, S.H., 1989. New technique applied to 3D seismic interpretation in Jarn Yaphour Field, Abu Dhabi, UAE. *Society of Petroleum Engineers* Paper SPE-17994, p. 697-715.

Adlan, Q. and John, C M., 2023. Clumped isotope record of individual limestone fabrics: a potential method to constrain the timing of oil migration. *Chemical Geology*, **616**, 121245, 12 pp.

Adlan, Q., Kaczmarek, S.E., and John, C.M., 2023. Clumped isotope reordering and kinetic differences in co-Hosted calcite and dolomite minerals throughout burial diagenesis and exhumation. *Minerals*, **13**, 1466, https://doi.org/10.3390/min13121466, 26 pp.

Aharonov, E. and Katsman, R., 2009. Interaction between pressure solution and clays in stylolite development: insights from modelin. *American Journal of Science*, **309**, 607-632.

Al-Ansari, F., Konwar, L.S., Urasaki, D., Parker, A., Hiraoka, T. and Mitsuishi, H., 2000. Vertical transmissibility assessment across stylolites in stratified carbonate reservoir – a field experience. *Society of Petroleum Engineers* Paper SPE-87301-MS, 10 pp.

Al-Ansi, H., Al-Wehaibi, M. and Stanley, R., 2012. Characterizing the relationship between petrophysical trends and diagenetic cementation patterns: a case study from the carbonate Arab C reservoir in the Dukhan Field, State of Qatar. *American Association of Petroleum Geologists Search and Discovery,* 90142, 1 pp.

Al Habsi, N., Al Shukaili, M., Al Tooqi, S., Ehrenberg, S.N. and Bernecker, M., 2014. Lithofacies, diagenesis and reservoir quality of Upper Shu'aiba reservoirs in northwestern Oman. *GeoArabia*, **19** (4), 145-182.

Al-Neyadi, A., Al Suwaidi, M.H., Deshpande, A., Ottinger, G., Edwards, H.E. and Akatsuka, K., 2012. Characterisation and geologic modeling of dolomitized burrows within a supergiant carbonate field, offshore Abu Dhabi. *American Association of Petroleum Geologists Search and Discovery*, 90141, 1 pp.

Ali, M., Watts, A. and Farid, A., 2014. Gravity anomalies of the United Arab Emirates: Implications for basement structures and infra-Cambrian salt distribution. *GeoArabia*, **19** (1), 85-112.

Ali, M.Y. and Farid, A., 2016. Cretaceous-Neogene structural evolution of SE Abu Dhabi, United Arab Emirates. *Journal of Petroleum Geology*, **39**, 221-246.

Al-Mansoori, A., Strohmenger, C.J., Abdul Ghani, A.A. and Mitchell, J.C., 2008. High-resolution sequence-stratigraphic correlation and facies characterization of upper Thamama (Lower Cretaceous) reservoir units and non-reservoir zones, Abu Dhabi, United Arab Emirates. *Society of Petroleum Engineers* Paper SPE-117905, 9 pp.

Alsharhan, A.S., 1985. Depositional environment, reservoir units evolution, and hydrocarbon habitat of Shuaiba Formation, Lower Cretaceous, Abu Dhabi, United Arab Emirates. *AAPG Bull.*, **69,** 899-912.

Alsharhan, A.S., 1990. Geology and reservoir characteristics of Lower Cretaceous Kharaib Formation in Zakum Field, Abu Dhabi, United Arab Emirates. In: Brooks, J. (Ed), Classic Petroleum Provinces. *Geol. Soc. London Special Publication* **50**, 299-316.

Alsharhan, A.S., 1993a. Asab Field - United Arab Emirates, Rub Al Khali Basin, Abu Dhabi. In: Foster, N.H. and Beaumont, E.A. (Eds), Structural Traps VIII. Treatise of Petroleum Geology, Atlas of Oil and Gas Fields, AAPG, Tulsa, 69-97.

Alsharhan, A.S., 1993b. Bu Hasa Field - United Arab Emirates, Rub Al Khali Basin, Abu Dhabi. In: Foster, N.H. and Beaumont, E.A. (Eds), Structural Traps VIII. Treatise of Petroleum Geology, Atlas of Oil and Gas Fields, AAPG, Tulsa, 99-127.

Alsharhan, A.S. and Sadd, J.L., 2000. Stylolites in Lower Cretaceous carbonate reservoirs, U.A.E. In: Alsharhan, A.S. and Scott, R.W. (Eds), Middle East Models of Jurassic/Cretaceous Carbonate Systems. *SEPM, Special Publications,* **69**, 185-207.

Alsharhan, A.S., Strohmenger, C.J. and Al-Mansoori, A., 2014. Mesozoic petroleum systems of Abu Dhabi, United Arab Emirates. In: Marlow, L., Kendall, C.C.G. and Yose, L.A. (Eds), Petroleum Systems of the Tethyan Region. *AAPG Memoir,* **106**, 679-711.

Alsuwaidi, M., Mansurbeg, H., Alsuwaidi, A., Morad, S., Mohamed, A.A., Amao, A.O. and Al-Ramadan, K., 2022. Comparison of diagenesis and reservoir quality of microporous lime mudstones (Aptian) between anticline crest and flanks: Abu

Dhabi, United Arab Emirates. *Marine and Petroleum Geology*, **145**, 105915, 14 pp.

Alteneiji, N., Denaro, M., Schlagintweit, F., Alsuwaidi, M., Hennhoefer, D. and Steuber, T., 2024. The Barremian – lower Aptian of NE Arabia: the Kharaib and Shu'aiba formations in Wadi Rahabah and Wadi Kebdah, Ras Al Khaimah, U.A.E. *Cretaceous Research*, **159**, 105873, 20 pp.

Arab, H., 1991. Bitumen occurrence and distribution in Upper Zakum Field. *Society of Petroleum Engineers* Paper SPE-21323, 146-165.

Arab, H., Mohamed, S. and Saltman, P., 1994. Facies controlled permeability variation in the Thamama II reservoir and its relationship to water breakthrough, Upper Zakum Field. Proceedings 6th Abu Dhabi International Petroleum Conference, ADSPE Paper **75**, 429-448.

Azer, S.R. and Toland, C., 1993. Sea level changes in the Aptian and Barremian (Upper Thamama) of offshore Abu Dhabi. *Society of Petroleum Engineers* Paper SPE-25610, 141-154.

Baldwin, B. and Butler, C.O., 1985. Compaction curves. *AAPG Bull.*, **69**, 622-626.

Barata, J., Vahrenkamp, V., Van Laer, P.J., Swart, P. and Murray, S., 2015. A regional analysis of clumped isotope geochemistry to define the timing of creation of micro-porosity in a Lower Cretaceous giant reservoir. *Society of Petroleum Engineers* Paper SPE-177922, 10 pp.

Bjørkum, P.A., Oelkers, E.H., Nadeau, P.H., Walderhaug, O. and Murphy, W.M., 1998. Porosity prediction in quartzose sandstones as a function of time, temperature, depth, stylolite frequency, and hydrocarbon saturation. *AAPG Bull.*, **82**, 637-648.

Bjørlykke, K., Mo, A. and Palm, E., 1988. Modelling of thermal convection in sedimentary basins and its relevance to diagenetic reactions. *Marine and Petroleum Geology*, **5,** 338-351.

Bjørlykke, K. and Jahren, J., 2012. Open or closed geochemical systems during diagenesis in sedimentary basins: constraints on mass transfer during diagenesis and the prediction of porosity in sandstone and carbonate reservoirs. *AAPG Bull.*, **96**, 2193-2214.

Boichard, R.A.P., Al-Suwaidi, A.S. and Karakhanian, H., 1994. Sequence boundary types and related porosity evolutions: example of the Upper Thamama Group in field "A" offshore Abu Dhabi, United Arab Emirates. In: Al-Husseini, I.M. (Ed), *GEO '94,* Gulf PetroLink, Bahrain, **1,** 191-201.

Braithwaite, C.J.R., 1989. Stylolites as open fluid conduits. *Marine and Petroleum Geology,* **6**, 93-96.

Brantferger, K.M., Kompanik, G.S., Al-Jenaibi, H.M., Dodge, W.S. and Patel, H., 2012. Impact and lessons of using high permeability streaks in history matching a giant offshore Middle East carbonate reservoir. *Society of Petroleum Engineers* Paper SPE-161426-MS, 7 pp.

Brasher, J.E. and Vagle, K.R., 1996. Influence of lithofacies and diagenesis on Norwegian North Sea chalk reservoirs. *AAPG Bull.*, **80**, 746-769.

Bruna, P.-O., Lavenu, A.P.C., Matonti, C. and Bertotti, G., 2019. Are stylolites fluid-flow efficient features? *Journal of Structural Geology*, **125**, 270-277.

Budd, D.A., 1989. Micro-rhombic calcite and microporosity in limestones: a geochemical study of the Lower Cretaceous Thamama Group, U.A.E. *Sedimentary Geology*, **63**, 293-311.

Bushara, M.N. and Arab, H.M., 1998. Fracture/stylolite characterization using stochastic modeling in zone-II reservoir, offshore Abu Dhabi. *Society of Petroleum Engineers* Paper SPE-49448-MS, 9 pp.

Carvalho, Á., Dias, A. and Ribeiro, M.T., 2011. Oil recovery enhancement for Thamama B lower in an onshore Abu Dhabi field. using conceptual models to understand reservoir behaviour. *Society of Petroleum Engineers*, SPE-148268-MS,

Clark, A., Stenger, B.A., Vahrenkamp, V., Al Dayyani, T. and Souliman, A., 2010. Improved description of shallow shelf-carbonates with resistivity-based imaging while drilling, Abu Dhabi, U.A.E. *Society of Petroleum Engineers* Paper SPE-137063-MS, 22 pp.

Cochard, J., Léonide, P., Borgomano, J., Guglielmi, Y., Massonnat, G., Rolando, J.-P., Marié, L. and Pasquier, A., 2020. Reservoir properties of Barremian – Aptian Urgonian limestones, SE France, Part 1: Influence of structural history on porosity-permeability variations. *Journal of Petroleum Geology*, **43**, 75-94.

Cochard, J., Léonide, P., Borgomano, J., Guglielmi, Y., Massonnat, G., Rolando, J.-P., Marié, L. and Pasquier, A., 2021. Reservoir properties of Barremian – Aptian Urgonian limestones, SE France, Part 2: Influence of diagenesis and fracturing. *Journal of Petroleum Geology,* **44**, 97-114.

Cox, P.A., Wood, R.A., Dickson, J.A.D., Al Rougha, H.B., Shebl, H. and Corbett, P.W.M., 2010. Dynamics of cementation in response to oil charge: evidence from a Cretaceous carbonate field, U.A.E. *Sedimentary Geology*, **228**, 246-254.

Cross, N.E., Singh, S.K., Al-Enezi, A. and S. Behbehani, S., 2022, Mixed carbonate-clastic reservoir characterization of the mid-Cretaceous Mauddud Formation (Albian), north Kuwait – implications for field development. *AAPG Bull.*, **106**, 289-319.

Czerniakowski, L.A., Lohmann, K.C. and Wilson, J.L., 1984. Closed-system marine burial diagenesis: isotopic data from the Austin Chalk and its components. *Sedimentology*, **31**, 863-877.

Davies, R.B., Casey, D.M., Horbury, A.D., Sharland, P.R. and Simmons, M.D., 2002. Early to mid-Cretaceous mixed carbonate-clastic shelfal systems: examples, issues and models from the Arabian Plate. *GeoArabia*, **7** (3), 541-598.

Droste, H.J., 2010. Sequence-stratigraphic framework of the Aptian Shu'aiba Formation in the Sultanate of Oman. In: van Buchem, F.S.P., Al-Husseini, M.I., Maurer, F. and Droste, H.J. (Eds), Aptian Stratigraphy and Petroleum Habitat of the Eastern Arabian Plate. *GeoArabia Special Publication* **4,** 1, 229-283.

Dujoncquoy, E., Grelaud, C., Razin, P., Imbert, P., van Buchem, F. Dupont, G. and Le Bec, A., 2018. Seismic stratigraphy of a Lower Cretaceous prograding carbonate platform (Oman) and implications for the eustatic sealevel curve. *AAPG Bull.*, **102**, 509-543.

Dunham, R.J., 1962. Classification of carbonate rocks according to depositional texture. In: Ham, W.E. (Ed), Classification of Carbonate Rocks. *AAPG Memoirs*, **1**, 108-121.

Eberli, G.P., Massaferro, J.L., Fonesca, C., Grötsch, J. and Asab Asset Team, 2001. Calibration of high-resolution sequence stratigraphy with FMI data: an example from the Thamama Group, Asab Field, Abu Dhabi. *AAPG Search and Discovery,* 90906, 1 pp.

Ehrenberg, S.N., Aqrawi, A.A.M. and Nadeau, P.H., 2008. An overview of reservoir quality in producing Cretaceous strata of the Middle East. *Petroleum Geoscience*, **14**, 307-318.

Ehrenberg, S.N., Walderhaug, O. and Bjørlykke, K., 2012. Carbonate porosity creation by mesogenetic dissolution: reality or illusion? *AAPG Bull.*, **96**, 217-233.

Ehrenberg, S. N., Morad, S., Yaxin, L. and R. Chen, R., 2016. Stylolites and porosity in a Lower Cretaceous limestone reservoir, onshore Abu Dhabi. *Journal of Sedimentary Research*, **86,** 1228-1247.

Ehrenberg, S.N., Lokier, S.W., Yaxin, L. and Chen, R., 2018. Depositional cycles in a Lower Cretaceous limestone reservoir, onshore Abu Dhabi, U.A.E. *Journal of Sedimentary Research*, **88**, 753-776.

Ehrenberg, S.N. and Wu, Q., 2019. Dense zones of the Kharaib Formation (Lower Cretaceous), United Arab Emirates. *Journal of Sedimentary Research*, **89**, 353-380.

Ehrenberg, S. N., 2019. Petrophysical heterogeneity in a Lower Cretaceous limestone reservoir, onshore Abu Dhabi, United

Arab Emirates. *AAPG Bull.*, **103**, 527-546.
Ehrenberg, S.N. and Baek, H., 2019. Deposition, diagenesis and reservoir quality of an Oligocene reefal-margin limestone succession: Asmari Formation, United Arab Emirates. *Sedimentary Geology,* **393-394**, 105535, 21 pp.
Ehrenberg, S.N., Zhang, J. and Gomes, J.S., 2020a. Regional porosity variation in Thamama-B reservoirs of Abu Dhabi. *Marine and Petroleum Geology*, **114**, 104245.
Ehrenberg, S.N., Zhang, J.. and Gomes, J.S.. 2020b. Regional variation of permeability in Thamama-B reservoirs of Abu Dhabi. *Marine and Petroleum Geology*, **116**, 104248.
Ehrenberg, S.N., 2022. The etiology of carbonate porosity. *AAPG Bull.*, **106**, 2351–2386.
Ehrenberg, S.N., Galluccio, L., Kostic, B., Bertouche, M., Frijia, G., Abd El-Aziz, S., Alabboud, N.E. and Ramalingam, R., *in preparation*. Porosity and permeability of Mauddud reservoirs in Raudhatain and Sabiriyah oilfields, Kuwait: description and interpretation of controlling processes.
Eilrich, B. and Grötsch, J., 2003. The Lower Cretaceous carbonate slope-to-platform-margin succession near Khatt, United Arab Emirates: sedimentary facies and depositional geometries. *GeoArabia,* **8**, 275-294.
Embry, A.F. and Klovan, J.E., 1971. A Late Devonian reef tract on northeastern Banks Island, N.W.T. *Bull. Canadian Petroleum Geol.*, **19**, 730-781.
Fox, A.F. and Brown, R.C.C., 1968. The geology and reservoir characteristics of the Zakum oil field, Abu Dhabi. *2nd AIME Regional Technical Symposium*, Saudi Arabia, 39-65.
Friedman, I., and O'Neil, J.R., 1977. Compilation of stable isotope fractionation factors of geochemical interest: Data of geochemistry, sixth edition: Washington, D.C. *United States Geological Survey Professional Paper* 440-KK, 12 pp.
Fullmer, S.M., Guidry, S.A., Gournay, J., Bowlin, E., Ottinger, G., Al Neyadi, A., Gupta, G., Gao, B. and Edwards, E., 2014. Microporosity: characterization, distribution, and influence on oil recovery. *Society of Petroleum Engineers* Paper SPE-171940, 17 pp.
Fullmer, S., Qassab, H.A., Buono, A., Gao, B., Kelley, B. and Moore, P.J., 2019. Carbonate pore-system influence on hydrocarbon displacement and potential recovery. In: McNeill, D.F, Harris, P.M., Rankey, E.C. and Hsieh, J.C.C. (Eds), Carbonate Pore Systems: New Developments and Case Studies. *SEPM Special Publications*, **112**, 268-284.
Gatel, P., Borgomano, J., Kenter, J. and Mecheri, T., 2024. Facies partitioning at regional and field scales in the Barremian Kharaib-2 Carbonates, UAE. *Journal of Petroleum Geology*, **47**, (4), 347-372.
Giles, M.R., 1997. *Diagenesis: a Quantitative Perspective Implications for Basin Modelling and Rock Property Prediction*, Dordrecht, Kluwer Academic Publishers, 526 pp.
Goldstein, R.H. and Reynolds, T.J., 1994. Systematics of fluid inclusions in diagenetic minerals. *SEPM Short Course* **31**, 199 pp.
Gomez-Rivas, E., Bons, P.D., Koehn, D., Urai, J.L., Arndt, M., Virgo, S., Laurich, B., Zeeb, C., Stark, L. and Blum, P., 2014. The Jabal Akhdar dome in the Oman Mountains: evolution of a dynamic fracture system. *American Journal of Science*, **314**, 1104-1139.
Gomez-Rivas, E., Martín-Martín, J.D., Bons, P.D., Koehn, D., Griera, A., Trav´e, A., Llorens, M.-G., Humphrey, E. and Neilson, J., 2022. Stylolites and stylolite networks as primary controls on the geometry and distribution of carbonate diagenetic alterations. *Marine and Petroleum Geology*, **136**, 105444, 14 pp.
Gran, K., Bjørlykke, K. and Aagaard, P., 1992. Fluid salinity and dynamics in the North Sea and Haltenbanken basins derived from well log data. In: Hurst, A., Griffiths, C.M. and Worthington, P.F. (Eds), Geological Applications of Wireline Logs II. *Geol. Soc. London Special Publication*, **65**, 327-338.
Grelaud, C., Razin, P., Vahrenkamp, V.C., Popa, D., Al Katheeri, F., Van Laer, P. and Leyrer, K., 2012. Stratigraphic architecture of the latest Jurassic - Early Cretaceous carbonate platform system of Abu Dhabi, United Arab Emirates (UAE). *Fourth Arabian Plate Geology Workshop, Late Jurassic/Early Cretaceous Evaporite-Carbonate-Siliciclastic Systems of the Arabian Plate*, 9-12 December 2012, Abu Dhabi, UAE, 3 pp.
Grötsch, J., Al-Jelani, O. and Al-Mehairi, Y., 1998. Integrated reservoir characterisation of a giant Lower Cretaceous oil field, Abu Dhabi, U.A.E. *Society of Petroleum Engineers* Paper SPE-49454, 77-86.
Gumati, Y., 1993. Kinetic modelling, thermal maturation and hydrocarbon generation in the United Arab Emirates. *Marine and Petroleum Geology*, **10**, 153-161.
Hanor, J.S. and Sassen, R., 1990. Evidence for large-scale vertical and lateral migration of formation waters, dissolved salt, and crude oil in the Louisiana Gulf Coast. In: Schumacher, D. and Perkins, B.F. (Eds), Gulf Coast Oils and Gases: Their Characteristics, Origin, Distribution, and Exploration and Production Significance. *SEPM Gulf Coast Section Publications, Proceedings of the Ninth Annual Research Conference*, 283-296.
Harris, T.J., Hay, J.T.C. and Twombley, B.N., 1968. Contrasting limestone reservoirs in the Murban Field, Abu Dhabi. *Society of Petroleum Engineers of AIME, 2nd Regional Technical Symposium*, Dhahran, Saudi Arabia, 27-29 March, 149-182.
Hasiuk, F.J., Kaczmarek, S.E. and Fullmer, S.M., 2016. Diagenetic origins of the calcite microcrystals that host microporosity in limestone reservoirs. *Journal of Sedimentary Research*, **86**, 1163-1178.
Hassan, T.H., Wada, Y. and Couroneau, J.C., 1979. The geology and development of the Thamama Zone IV of the Zakum Field, Abu Dhabi. *Society of Petroleum Engineers* Paper SPE-7779, 231-246.
Hawas, M.F. and Takezaki, H., 1995. A model for migration and accumulation of hydrocarbons in the Thamama and Arab reservoirs in Abu Dhabi. In: Al-Husseini, M.I. (Ed.) *GEO'94, Middle East Petroleum Geosciences*, Gulf PetroLink, Bahrain, **2**, 483-495.
Heap, M.J., Baud, P., Reuschlé, T. and Meredith, P.G., 2014. Stylolites in limestones: barriers to fluid flow? *Geology*, **42**, 51-54.
Heasley, E.C., Worden, R.H. and Hendry, J.P., 2000. Cement distribution in a carbonate reservoir: recognition of a palaeo oil-water contact and its relationship to reservoir quality in the Humbly Grove Field, onshore, UK. *Marine and Petroleum Geology*, **17**, 639-654.
Heydari, E., 1997. Hydrotectonic models of burial diagenesis in platform carbonates based on formation water geochemistry in North American sedimentary basins. In: Montanez, I.P., Gregg, J.M. and Shelton, K.L. (Eds), Basin-wide Diagenetic Patterns: Integrated Petrologic, Geochemical, and Hydrologic Considerations. *SEPM Special Publications*, **57**, 53–79.
Heydari-Farsani, E., Neilson, J.E., Alsop, G.I. and Hamidi, H., 2020. Tectonic controls on residual oil saturation below the present-day fluid contact level in reservoirs of the Persian Gulf. *Journal of Asian Earth Sciences*, 190, 104133, 14 pp.
Hillgärtner, H., van Buchem, F.S.P., Gaumet, F., Razin, P., Pittet, B., Grötsch, J. and Droste, H.J., 2003. The Barremian-Aptian evolution of the Eastern Arabian carbonate platform margin (northern Oman). *Journal of Sedimentary Research*, **73**, 756-773.
Hillgärtner, H., 2010. Anatomy of a microbially constructed, high-energy, ocean-facing carbonate platform margin (earliest Aptian, northern Oman Mountains). In: van Buchem, F.S.P., Al-Husseini, M.I., Maurer, F. and Droste, H.J. (Eds), Aptian Stratigraphy and Petroleum Habitat of the Eastern Arabian Plate. *GeoArabia Special Publication* **4**, 1, 285-300.
Hollis, C., Lawrence, D.A., Deville de Periere, M. and Al Darmaki, F., 2017. Controls on porosity preservation within a Jurassic oolitic reservoir complex, UAE. *Marine and Petroleum Geology*, **88**, 888-906.
Huck, S., Wohlwend, S., Coimbra, R., Christ, N. and Weissert, H.,

2017. Disentangling shallow-water bulk carbonate carbon isotope archives with evidence for multi-stage diagenesis: an in-depth component-specific petrographic and geochemical study. *The Depositional Record*, **3**, 233-257.

Immenhauser, A., Schlager, W., Burns, S.J., Scott, R.W., Geel, T., Lehmann, J., Van Der Gaast, S. and Bolder-Schrijver, L.J.A., 1999. Late Aptian to late Albian sea-level fluctuations constrained by geochemical and biological evidence (Nahr Umr Formation, Oman). *Journal of Sedimentary Research*, **69**, 434-446.

Immenhauser, A., Creusen, A., Esteban, M. and Vonhof, H., 2000. Recognition and interpretation of polygenetic disormity surfaces in the middle Cretaceous Shu'aiba, Nahr Umr, and Natih Formations of northern Oman. *GeoArabia*, **5** (2), 299-322.

Immenhauser, A., Hillgaertner, H., Sattler, U., Bertotti, G., Schoepfer, P., Homewood, P., Vahrenkamp, V., Steuber, T., Masse, J.-P., Droste, H., Taal-van Koppen, J., van der Kooij, B., van Bentum, E., Verwer, K., Strating, E.H., Swinkels, W., Peters, J., Immenhauser-Potthast, I. and Al Maskery, S., 2004. Barremian-lower Aptian Qishn Formation, Haushi-Huqf area, Oman: a new outcrop analogue for the Kharaib/Shu'aiba reservoirs. *GeoArabia*, **9** (1), 153-194.

Jayachandran, I.S.A.J., 2017. Nature of the Top-Thamama-B Surface in Field A, Onshore Abu Dhabi. *Unpublished Master of Science Dissertation*, Khalifa University of Science and Technology, 232 pp.

Johnson, J.A.D. and Budd, S.R., 1975. The geology of the zone B and zone C Lower Cretaceous limestone reservoirs of Asab Field, Abu Dhabi. *9th Arab Petroleum Congress*, Dubai, Paper **109** (B-3), 24 pp.

Kaczmarek, S.E., Fullmer, S.M. and Hasiuk, F.J., 2015. A universal classification scheme for the microcrystals that host limestone microporosity. *Journal of Sedimentary Research*, **85**, 1197-1212.

Khan, S.H., Nasir, W.A, El Sahn, H., Sudiro, H., AlWahedi, M.A., AlMazrooei, S.H., Lehmann, C., Ramos, L.M., Singh, M., Singh, M.K. and Al Ali, M.Y., 2021. Innovative high permeability streak characterization and modeling utilizing static and dynamic data in a complex giant mature oil field in the Middle East. *Society of Petroleum Engineers* Paper SPE-207310-MS, 19 pp.

Kharaka, Y.K. and Hanor, J.S., 2004. Deep fluids in the continents: I. sedimentary basins. In: Drever, J. I., Holland, H.D. and Turekian, K.K. (Eds), *Treatise on Geochemistry*, Elsevier, Amsterdam, **5**, 499-540.

Kim, S.-T. and O'Neil, J.R., 1997. Equilibrium and non-equilibrium oxygen isotope effects in synthetic carbonates. *Geochimica et Cosmochimica Acta*, 61, 3461-3475.

Kirkham, A., Bin Juma, M., McKean, T.A.M., Palmer, A.F., Smith, M.J., Thomas, A.H. and Twombley, B.N., 1996. Fluid saturation predictions in a "transition zone" carbonate reservoir, Abu Dhabi. *GeoArabia*, **1** (4), 551-566.

Koehn, D., Rood, M. P., Beaudoin, N., Chung, P., Bons, P. D. and Gomez-Rivas, E., 2016. A new stylolite classification scheme to estimate compaction and local permeability variations. *Sedimentary Geology,* **346**, 60-71.

Koepnick, R.B., 1987. Distribution and permeability of stylolite-bearing horizons within a Lower Cretaceous carbonate reservoir in the Middle East. *SPE Formation Evaluation*, **2** (2), 137-142.

Kristiansen, K., Valtiner, M., Greene, G.W., Boles, J.R. and Israelachvili, J.N., 2011. Pressure solution – the importance of the electrochemical surface potentials. *Geochimica et Cosmochimica Acta*, **75**, 6882-6892.

Lambert, L., Durleta, C., Loreau, J.-P. and Marnier, G., 2006. Burial dissolution of micrite in Middle East carbonate reservoirs (Jurassic – Cretaceous): keys for recognition and timing. *Marine and Petroleum Geology*, **23**, 79-92.

Land, L.S., 1983. The application of stable isotopes to studies of the origin of dolomite and to problems of diagenesis of clastic sediments. In: Arthur, M.A., Anderson, T.F., Kaplan, I.R., Veizer, J. and Land, L.S. (Eds), Stable Isotopes in Sedimentary Geology. *SEPM Short Course* **10**, 4-1 – 4-22.

Lehmann, C., Osleger, D.A. and Montañez, I., 2000. Sequence stratigraphy of Lower Cretaceous (Barremian-Albian) carbonate platforms of northeastern Mexico: regional and global correlations. *Journal of Sedimentary Research*, **70**, 373-391.

Le Nindre, Y. M., Vaslet, D., Le Metour, J., Bertrand, J. and Halawani, M., 2003. Subsidence modelling of the Arabian Platform from Permian to Paleogene outcrops. *Sedimentary Geology*, **156**, 263-285.

Liu, H., Shi, K., Liu, B., Li, Y., Li, Y., Zheng, H., Peng, Y. and Fu, Y., 2024. High-magnesium calcite skeletons provide magnesium for burrow-selective dolomitization in Cretaceous carbonates. *Sedimentology*, **71**, 383-418.

Lohmann, K.C., 1988. Geochemical pattern of meteoric diagenetic systems and their application to the studies of paleokarst. In: James, N.P. and Choquette, P.W. (Eds), Paleokarst. New York, Springer Verlag, 58-80.

Looser, N., Petschnig, P., Hemingway, J.D., Fernandez, A., Grafulha, L.M., Perez-Huerta, A., Vickers, M.L., Price, G.D., Schmidt, M.W. and Bernasconi, S.M., 2023. Thermally-induced clumped isotope resetting in belemnite and optical calcites: towards material-specific kinetics. *Geochimica et Cosmochimica Acta*, **350**, 1-15.

Loosveld, R.J.H., Bell, A. and Terken, J.J.M., 1996. The tectonic evolution of interior Oman. *GeoArabia*, **1** (1), 28-51.

Loucks, R. G. and Bebout, D.G., 1984. Shelf-interior carbonate grainstone shoals: Lower Cretaceous Pearsall Formation, south Texas. In: Harris, P.M. (Ed), Carbonate Sands: A Core Workshop. *SEPM Core Workshop* **5**, 334-364.

Lucia, F.J., 1995, Rock-fabric/petrophysical classification of carbonate pore space for reservoir characterization. *AAPG Bull.*, **79**, 1275-1300.

Madanipour, S., Najafi, M., Nozaem, R., Vergés, J., Yassaghi, A., Heydari, I., Khodaparast, S., Soudmand, Z. and Aghajari, L., 2024. The Arabia – Eurasia collision zone in Iran: tectonostratigraphic and structural synthesis. *Journal of Petroleum Geology*, **47**, 123-172.

Marquer, D., Peters, T. and Gnos, E., 1995. A new structural interpretation for the emplacement of the Masirah ophiolites (Oman): a main Paleocene intra-oceanic thrust. *Geodinamica Acta*, **8** (1), 13-19.

Martín-Martín, J.D., Gomez-Rivas, E., Gomez-Gras, D., Trave, A., Ameneiro, R., Koehn, D. and Bons, P.D., 2018. Activation of stylolites as conduits for overpressured fluid flow in dolomitized platform carbonates. In: Ashton, M., Dee, S.J. and Wennberg, O.P. (Eds), Subseismic-scale Reservoir Deformation. *Geol. Soc. London Special Publication* **459**, 157–176.

Marzouk, I. and El Sattar, M. A., 1994. Wrench tectonics in Abu Dhabi, United Arab Emirates. In: Al-Husseini, M.I. (Ed.), *Geo '94 The Middle East Petroleum Geosciences 1: Selected Papers from the Middle East Geoscience Conference*, Bahrain, 655-668.

Maurer, F., Al-Mehsin, K., Pierson, B.J., Eberli, G.P., Warrlich, G., Drysdale, D. and Droste, H.J., 2010. Facies characteristics and architecture of Upper Aptian Shu'aiba clinoforms in Abu Dhabi. In: van Buchem, F.S.P., Al-Husseini, M.I., Maurer, F. and Droste, H.J. (Eds), Aptian Stratigraphy and Petroleum Habitat of the Eastern Arabian Plate. *GeoArabia Special Publication* **4**, 2, 445-468.

Melville, P., Al Jeelani, O., Al Menhali, S. and Grötsch, J., 2004. Three-dimensional seismic analysis in the characterization of a giant carbonate field, onshore Abu Dhabi, United Arab Emirates. In: Eberli, G.P., Massaferro, J.L. and Sarg, J.F. (Eds), Seismic Imaging of Carbonate Reservoirs and Systems. *AAPG Memoirs*, **81**, 123-148.

Mohamed, A. and Ennadi, I., 1995. The origin of oil and gas in

onshore Abu Dhabi, UAE. *AAPG Bull.*, **79**, 1236-1237.
Morad, D., Paganoni, M., Al Harthi, A., Morad, S., Ceriani, A., Mansurbeg, H., Al Suwaidi, A., Al-Aasm, I.S. and Ehrenberg, S.N., 2016. Origin and evolution of microporosity in packstones and grainstones in a Lower Cretaceous carbonate reservoir, United Arab Emirates. In: Armitage, P.J., Butcher, A.R., Churchill, J.M., Csoma, A.E., Hollis, C., Lander, R.H., Omma, J.E. and Worden, R.H. (Eds), Reservoir Quality of Clastic and Carbonate Rocks: Analysis, Modelling and Prediction. *Geol. Soc. London Special Publications*, **435**, 1-36.
Morad, D., Nader, F.H., Gasparrini, M., Morad, S., Rossi, C., Marchionda, E., Al Darmaki, F., Martines, M. and Helge Hellevang, H., 2018. Comparison of the diagenetic and reservoir quality evolution between the anticline crest and flank of an Upper Jurassic carbonate gas reservoir, Abu Dhabi, United Arab Emirates. *Sedimentary Geology*, **367**, 96-113.
Morad, S., Al Suwaidia, M., Mansurbeg, H., Morad, D., Ceriani, A., Paganoni, M. and Al-Aasm, I., 2019. Diagenesis of a limestone reservoir (Lower Cretaceous), Abu Dhabi, United Arab Emirates: comparison between the anticline crest and flanks. *Sedimentary Geology*, **380**, 127-142.
Murad, A.A., Garamoon, H., Hussein, S. and Al-Nuaimi, H.S., 2011. Hydrogeochemical characterization and isotope investigations of a carbonate aquifer of the northern part of the United Arab Emirates. *Journal of Asian Earth Sciences*, **40**, 213-225.
Murris, R.J., 1980. Middle East: stratigraphic evolution and oil habitat. *AAPG Bull.*, **64**, 597-618.
Nadeau, P.H., Sun, S. and Ehrenberg, S.N., 2023. The "Golden Zone" temperature distribution of oil and gas occurrence examined using a global empirical database. *Marine and Petroleum Geology*, **158,** 106507, 20 pp.
Neilson, J.E., Oxtoby, N.H. and Simmons, M.D., 1996. Effect of petroleum emplacement on reservoir quality in the Thamama reservoirs of Abu Dhabi. *Society of Petroleum Engineers* Paper SPE-36241, 12 p.
Neilson, J.E., Oxtoby, N.H., Simmons, M.D., Simpson, I.R. and Fortunatova, N.K., 1998. The relationship between petroleum emplacement and carbonate reservoir quality: examples from Abu Dhabi and the Amu Darya Basin. *Marine and Petroleum Geology*, **15,** 57-72.
Neilson, J.E. and Oxtoby, N.H., 2008. The relationship between petroleum, exotic cements and reservoir quality in carbonates - a review. *Marine and Petroleum Geology*, **25**, 778-790.
O'Brien, C.L., Robinson, S.A., Pancost, R.D., Damste, J.S.S., Schouten, S., Lunt, D.J., Alsenz, H., Bornemann, A., Bottini, C. and Brassell, S.C., 2017. Cretaceous sea-surface temperature evolution: constraints from TEX86 and planktonic foraminiferal oxygen isotopes. *Earth-Science Reviews*, **172**, 224–247.
Ottinger, G., Kompanik, G., Al Suwaidi, M., Brantferger, K. and Edwards, H., 2012. Integration of subsurface data, modern analog concepts, and history matching feedback to model a thick carbonate reservoir, offshore Abu Dhabi. *Society of Petroleum Engineers* Paper SPE-161715-MS, 20 pp.
Oswald, E J., Mueller III, H.W., Goff, D.F., Al-Habshi, H. and Al Matroushi, S., 1995. Controls on porosity evolution in Thamama Group carbonate reservoirs in Abu Dhabi, U.A.E. *Society of Petroleum Engineers* Paper SPE-029797-MS, 251-265.
Paganoni, M., Al Harethi, A., Morad, D., Morad, S., Ceriani, A., Mansurbeg, H., Al Suwaidi, A., Al-Aasm, I.S., Ehrenberg, S.N. and Sirat, M., 2016. Impact of stylolitization on diagenesis of a Lower Cretaceous carbonate reservoir from a giant oilfield, Abu Dhabi, United Arab Emirates. *Sedimentary Geology*, **335**, 70–92.
Perrin, C., Marquez, X., Flores, J. and Berthereau, G., 2020. Porosity Depth Saturation (PDS) model: quantification of porosity preservation with burial in carbonate oil reservoirs, and application to infer oil charging time. *Marine and Petroleum Geology*, **120**, 104515, 14 pp.
Pierson, B., Eberli, G., Al-Mehsin, K., Al-Menhali, S., Warrlich, G., Droste, H., Maurer, F., Whitworth, J. and Drysdale, D., 2010. Seismic stratigraphy and depositional history of the Upper Shu'aiba (Late Aptian) in the UAE and Oman. In: van Buchem, F.S.P., Al-Husseini, M.I., Maurer, F. and Droste, H.J. (Eds), Aptian Stratigraphy and Petroleum Habitat of the Eastern Arabian Plate. *GeoArabia Special Publication* **4**, 2, 411-444.
Pittet, B., van Buchem, F., Hillgaertner, H., Grötsch, J. and Droste, H., 2002. Ecological succession, palaeonvironmental change, and depositional sequences of Barremian-Aptian shallow-water carbonates in northern Oman. *Sedimentology*, **49**, 555-581.
Pontes, C.C.C., Balsamo, F., Pizzati, M., Bezerra, F.H., La Bruna, V. and Lima, R.S., 2023. Burial stylolites enhance karst dissolution and control cave geometry in heterolithic carbonates, Salitre Formation, Brazil. *Marine and Petroleum Geology*, **148**, 106029, 18 pp.
Prezbindowski, D. R., 1985. Burial cementation - is it important? A case study, Stuart City trend, south central Texas. In: Schneidermann, N. and Harris, P.M. (Eds), Carbonate Cements. *SEPM Special Publications*, **36**, 241-264.
Rameil, N., Immenhauser, A., Csomo, A.E. and Warrlich, G., 2012. Surfaces with a long history: the Aptian top Shu'aiba Formation unconformity, Sultanate of Oman. *Sedimentology*, **59,** 212-248.
Raven, M.J. and Dickson, J.A.D., 2007. Methanogenesis during Shu'aiba diagenesis: examples from Al Shaheen Field, Block 5, offshore Qatar. *GeoArabia*, **12** (1), 37-58.
Razin, P., Grélaud, C., Dujoncquoy, E. and Lebec, A., 2013. Latest Jurassic to early Barremian carbonate systems from the United Arab Emirates to Oman: regional stratigraphic architecture and controlling factors. *GeoArabia*, **18** (2), 241-245.
Rousseau, M., Dromart, G., Garcia J.P., Atrops, F. and Guillocheau, F., 2005. Jurassic evolution of the Arabian carbonate platform edge in central Oman Mountains. *Journal of the Geological Society,* **162**, 349-362.
Rousseau, M., Dromart, G., Droste, H., and Homewood, P., 2006. Stratigraphic organisation of the Jurassic sequence in Interior Oman, Arabian Peninsula. *GeoArabia*, **11** (1), 17-50.
Saotome, J.-I., Shibasaki, T., Shikama, T. and Kawaguchi, K.I., 2000. Geological controls on pore geometry of upper Kharaib reservoir, offshore Abu Dhabi, U.A.E. In: Alsharhan, A.S. and Scott, R.W. (Eds), Middle East Models of Jurassic/Cretaceous Carbonate Systems *SEPM Special Publications*, **69**, 287-297.
Sattler, U., Immenhauser, A., Hillgartner, H. and Esteban, M., 2005. Characterization, lateral variability and lateral extent of discontinuity surfaces on a Carbonate Platform (Barremian to Lower Aptian, Oman). *Sedimentology*, **52**, 339-361.
Scharf, A., Mattern, F., Al-Wardi, M., Frijia, G., Moraetis, D., Pracejus, B., Bauer, W. and Callegari, I., 2021. Chapter 5. Tectonic evolution of the Oman Mountains. In: Scharf, A., Mattern, F., Al-Wardi, M., Frijia, G., Moraetis, D., Pracejus, B., Bauer, W. and Cellegari, I. (Eds), The Geology and Tectonics of the Jabal Akhdar and Saih Hatat Domes, Oman Mountains. *Geol. Soc. London Memoirs*, **54**, 67–103.
Schlagintweit, F., Alteneiji, N., and Steuber, T., 2024. Voloshinoides simplex sp. nov. and Cribellopsis? kharaibensis sp. nov. (Foraminifera): new constraints for Lower Cretaceous (upper Barremian–lowermost Aptian) stratigraphy of the Arabian Plate (Kharaib Formation, Hawar Member, UAE): *Revue de micropaléontologie*, **83**, 100785, 9 pp.
Schmoker, J.W. and Halley, R.B., 1982. Carbonate porosity versus depth: a predictable relation for south Florida. *AAPG Bull.*, **66**, 2561-2570.
Schmoker, J.W., 1984. Empirical relation between carbonate porosity and thermal maturity: an approach to regional

porosity prediction. *AAPG Bull.*, **68**, 1697-1703.

Schreurs, G. and Immenhauser, A., 1999. West-northwest directed obduction of the Batain Group on the eastern Oman continental margin at the Cretaceous – Tertiary boundary. *Tectonics*, **18**, 148-160.

Schroeder, R., van Buchem, F.S.P., Cherchi, A., Baghbani, D., Vincent, B., Immenhauser, A. and Granier, B., 2010. Revised orbitolinid biostratigraphic zonation for the Barremian – Aptian of the eastern Arabian Plate and implications for regional stratigraphic correlations. In: van Buchem, F.S.P., Al-Husseini, M.I., Maurer, F. and Droste, H.J. (Eds), Aptian Stratigraphy and Petroleum Habitat of the Eastern Arabian Plate. *GeoArabia Special Publication* **4**, 1, 49-96.

Sharland, P.R., Archer, R., Casey, D.M., Davies, R.B., Hall, S.H., Heward, A.P., Horbury, A.D. and Simmons, M.D., 2001. Arabian plate sequence stratigraphy. *GeoArabia Special Publication* **2**, 371 pp.

Shekhar, R., Al Naqbi, A., Obeta, C., Ottinger, G., Herrmann, R., Obara, T., Almazrouei, S.J., Maqrami, Z.N., Al Neyadi, A., Edwards, E., Shebl, H., Li, D., Shehhi, B.H. and Fazal, A., 2017. Implementation of high resolution diagenetic features into the static and dynamic reservoir models of a giant offshore oil field, Abu Dhabi. *Society of Petroleum Engineers* Paper SPE-188872-MS, 16 pp.

Shekhar, R., Edwards, E. and Obeta, C., 2019. Review of identification, characterization and modeling of different types of fault & fracture systems in a giant offshore carbonate reservoir, UAE. *Society of Petroleum Engineers* Paper SPE-197547-MS, 13 pp.

Skene, K.I., Yamamoto, K., Brantferger, K, Quintero, M., Kompanik, G., Ottinger, G. and Al Harbi, M., 2014. Accounting for multi-scale permeability systems in reservoir models of a giant offshore oil field, Abu Dhabi – balancing matrix versus excess permeability and its impact on reservoir performance. *Society of Petroleum Engineers* Paper SPE-171876-MS, 12 pp.

Soreghan, G.S., 1997. Walther's Law, climate change, and Upper Paleozoic cyclostratigraphy in the ancestral Rocky Mountains. *Journal of Sedimentary Research*, **67**, 1001-1004

Sprovieri, M., Coccioni, R., Lirer, F., Pelosi, N. and Lozar, F., 2006. Orbital tuning of a Lower Cretaceous composite record (Maiolica Formation, central Italy). *Paleooceanography*, **21**, PA4212, doi:10.1029/2005PA001224, 19 pp.

Stenger, B.A., Al-Katheeri, A.B., Hafez, H.H. and Al-Kendi, S.H., 2008. Short-term and long-term aspects of a water injection strategy. *SPE Reservoir Evaluation and Engineering*, December, 841-852.

Steuber, T., Alsuwaidi, M., Hennhoefer, D., Sulieman, H., Al Blooshi, A., McAlpin T.D. and Shebl, H., 2022. Environmental change and carbon-cycle dynamics during the onset of Cretaceous oceanic anoxic event 1a from a carbonate-ramp depositional system, Abu Dhabi, U.A.E. *Palaeogeography, Palaeoclimatology, Palaeoecology*, **601**, 111086, 11 pp.

Strohmenger, C.J., Weber, L.J., Ghani, A., Al-Mehsin, K., Al-Jeelani, O., Al-Mansoori, A., Al-Dayyani, T., Vaughan, L., Khan S.A. and Mitchell, J.C., 2006. High-resolution sequence stratigraphy and reservoir characterization of upper Thamama (Lower Cretaceous) reservoirs of a giant Abu Dhabi oil field, United Arab Emirates. In: Harris, P.M. and Weber, L.J. (Eds), Giant Hydrocarbon Reservoirs of the World: From Rocks to Reservoir Characterization and Modeling. *AAPG Memoirs*, **88**, 139-171.

Strohmenger, C.J., Steuber, T., Ghani, A., Barwick, D.G., Al-Mazrooei, S.H.A. and Al-Zaabi, N.O., 2010. Sedimentology and chemostratigraphy of the Hawar and Shu'aiba depositional sequences, Abu Dhabi, United Arab Emirates. In: van Buchem, F.S.P., Al-Husseini, M.I., Maurer, F. and Droste, H.J. (Eds), Aptian Stratigraphy and Petroleum Habitat of the Eastern Arabian Plate. *GeoArabia Special Publication* **4**, 2, 341-365.

Taher, A.A., 1997. Delineation of organic richness and thermal history of the Lower Cretaceous Thamama Group, east Abu Dhabi: a modeling approach for oil exploration. *GeoArabia*, **2** (1), 65-88.

Taher, A., 2019. Hydrocarbon exploration potential in migration pathways. *Society of Petroleum Engineers* Paper SPE-123456-MS, 14 pp.

Taylor, T. R., Giles, M.R., Hathon, L.A., Diggs, T.N., Braunsdorf, N.R., Birbiglia, G.V., Kittridge, M.G., Macaulay, C.I. and Espejo, I.S., 2010. Sandstone diagenesis and reservoir quality prediction: models, myths, and reality. *AAPG Bull.*, **94**, 1093-1132.

Tendil, A.J.-B., Frau, C., Leonide, P., Fournier, F., Borgomano, J.R., Lanteaume, C., Masse, J.-P., Massonnat, G. and Rolando, J.-P., 2018. Platform-to-basin anatomy of a Barremian-Aptian Tethyan carbonate system: new insights into the regional to global factors controlling the stratigraphic architecture of the Urgonian Provence platform (southeast France). *Cretaceous Research*, **91**, 382-411.

Tendil, A.J.-B., Frau, C., Leonide, P., Fournier, F., Borgomano, J.R., Lanteaume, C., Masse, J.-P. and Rolando, J.-P., 2019. Chapter five: Stable-isotope chemostratigraphy of Urgonian-type platform carbonates: time to be cautious? In: Montenarri, M. (Ed), *Case Studies in Isotope Stratigraphy, Stratigraphy and Time Scales* **4**. Elsevier, 165-216.

Tendil, A.J.-B., Galluccio, L., Breislin, C., Alsabeai, J.E., Lavenu, A.P.C. and Obara, A., 2021. New insights on the lower Lekhwair Formation (offshore Abu Dhabi): understanding the key role of *Lithocodium*/*Bacinella* floatstones on large scale reservoir quality variations. *Society of Petroleum Engineers* Paper SPE-207692.

Tendil, A.J.-B., Hatter, S.J., Galluccio, L., Breislin, C., Al-Shamsi, S.G., Syofyan, S., Bal Baheeth, A.H.A., Adlan, F., Raina, I. and Mansour, B., 2022. Understanding reservoir heterogeneities in a Lower Cretaceous Thamama reservoir. *Society of Petroleum Engineers* Paper SPE-211678-MS, 16 pp.

Thomas, M. and Heine, C., 2019. Setting the scene for a Paleogene clastic basin; obduction of the Masirah Ophiolite, Oman. *AAPG Search and Discovery*, 90360, 1 pp.

Vahrenkamp, V.C., 1996. Carbon isotope stratigraphy of the Upper Kharaib and Shuaiba Formations: implications for the Early Cretaceous evolution of the Arabian Gulf Region. *AAPG Bull.*, **80**, 647-662.

Vahrenkamp, V. C., 2010. Chemostratigraphy of the Lower Cretaceous Shu'aiba Formation: a $\delta^{13}C$ reference profile for the Aptian Stage from the southern Neo-Tethys Ocean. In: van Buchem, F.S.P., Al-Husseini, M.I., Maurer, F. and Droste, H.J. (Eds), Aptian Stratigraphy and Petroleum Habitat of the Eastern Arabian Plate. *GeoArabia Special Publication* **4**, 1, 107-137.

Vahrenkamp, V., Barata, J., Van Laer, P.J., Swart, P. and Murray, S., 2014. Micro-rhombic calcite of a giant Barremian (Thamama B) reservoir onshore Abu Dhabi - clumped isotope analyses fix temperature, water composition and timing of burial diagenesis. *Society of Petroleum Engineers* Paper SPE-172033, 12 pp.

Vahrenkamp, V.C., Van Laer, P., Franco, B., Celentano, M.A., Grelaud, C. and Razin, P., 2015. Late Jurassic to Cretaceous source rock prone intra-shelf basins of the eastern Arabian Plate – interplay between tectonism, global anoxic events and carbonate platform dynamics. *International Petroleum Technology Conference*, Doha, Qatar, 7–9 December, IPTC-18470-MS, 24 pp.

Van Breugel, Y., Schouten, S., Tsikos, H., Erba, E., Price, G.D. and Damsté, J.S.S., 2007. Synchronous negative carbon isotope shifts in marine and terrestrial biomarkers at the onset of the Early Aptian oceanic anoxic event 1a: evidence for the release of ^{13}C-depleted carbon into the atmosphere. *Paleoceanography*, **22**, PA1210.

van Buchem, F.S.P., Pittet, B., Hillgartner, H., Grötsch, J., Al

Mansouri, A.I., Billing, I.M., Droste, H.H.J., Oterdoom, W.H. and van Steenwinkel, M., 2002. High-resolution sequence stratigraphic architecture of Barremian/Aptian carbonate systems in northern Oman and the United Arab Emirates (Kharaib and Shu'aiba formations). *GeoArabia*, **7** (3), 461-500.
van Buchem, F.S.P., Al-Husseini, M.I., Maurer, F., Droste, H.J. and Yose, L.A., 2010a. Sequence-stratigraphic synthesis of the Barremian – Aptian of the eastern Arabian Plate and implications for the petroleum habitat. In: van Buchem, F.S.P., Al-Husseini, M.I., Maurer, F. and Droste, H.J. (Eds), Aptian Stratigraphy and Petroleum Habitat of the Eastern Arabian Plate. *GeoArabia Special Publication* **4**, 1, 9-48.
van Buchem, F.S.P., Baghbani, D., Bulot, L.G., Caron, M., Gaumet, F., Hosseini, A., Keyvani, F., Schroeder, R., Swennen, R., Vedrenne, V. and Vincent, B., 2010b. Barremian – Lower Albian sequence stratigraphy of southwest Iran (Gadvan, Dariyan and Kazhdumi formations) and its comparison with Oman, Qatar and the United Arab Emirates. In: van Buchem, F.S.P., Al-Husseini, M.I., Maurer, F. and Droste, H.J. (Eds), Aptian Stratigraphy and Petroleum Habitat of the Eastern Arabian Plate. *GeoArabia Special Publication* **4,** 2, 503-548.
Van Simaeys, S., Rendall, B., Lucia, F.J., Kerans, C. and Fullmer, S., 2017. Facies-independent reservoir characterization of the micropore-dominated Word field (Edwards Formation), Lavaca County, Texas. *AAPG Bull.*, **101**, 73–94.
Vaughan, R.L., Khan, S.A., Weber, L.J., Suwaina, O., Al-Mansoori, A., Ghani, A., Strohmenger, C.J., Herrmann, M.A. and Hulstrand, D., 2004. Integrated characterization of UAE outcrops: From rocks to fluid flow simulation. *Society of Petroleum Engineers* Paper SPE-88730, 17 pp.
Veizer, J., Ala, D., Azamy, K., Bruckschen, P., Buhl, D., Bruhn, F., Carden, G.A.F. Deiner, A., Ebneth, S., Godderis, Y., Jasper, T., Korte, C., Pwallek, F., Podlaha, O.G. and Strauss, H., 1999. $^{87}Sr/^{86}Sr$, $\delta^{13}C$ and $\delta^{18}O$ evolution of Phanerozoic seawater. *Chemical Geology*, **161**, 59-88.
Wagner, P.D., 1990. Geochemical stratigraphy and porosity controls in Cretaceous carbonates near the Oman Mountains. In: Robertson, A.H.F., Searle, M.P. and Ries, A.C. (Eds), The Geology and Tectonics of the Oman Region. *Geol. Soc. London Special Publication* **49**, 127-137.
Walderhaug, O., Bjørkum, P.A. and Aase, N.E., 2006. Kaolin-coating of stylolites, effect on quartz cementation and general implications for dissolution at mineral interfaces. *Journal of Sedimentary Research*, **76**, 234-243.
Walderhaug, O., 1996. Kinetic modeling of quartz cementation and porosity loss in deeply buried sandstone reservoirs. *AAPG Bull.*, **80**, 731-745.
Wang, P., Wang, G., Chen, Y., Hao, F., Yang, X., Hu, F., Zhou, L., Yi, Y., Yang, G., Wang, X. and Cong, F., 2023. Formation and preservation of ultra-deep high-quality dolomite reservoirs under the coupling of sedimentation and diagenesis in the central Tarim Basin, NW China. *Marine and Petroleum Geology*, **149**, 106084, 14 pp.
Wanless, H.R. and Tagett, M.G., 1989. Origin, growth and evolution of carbonate mudbanks in Florida Bay. *Bull. Marine Science*, **44,** 454-489.
Warrlich, G., Hillgartner, H., Rameil, N., Gittins, J., Mahruqi, I., Johnson, T., Alexander, D., Wassing, B., Van Steenwinkel, M. and Droste, H.J., 2010. Reservoir characterisation of data-poor fields with regional analogues: A case study from the Lower Shu'aiba in the Sultanate of Oman. In: van Buchem, F.S.P., Al-Husseini, M.I., Maurer, F. and Droste, H.J. (Eds), Aptian Stratigraphy and Petroleum Habitat of the Eastern Arabian Plate. *GeoArabia Special Publication* **4**, 2, 577-604.
Wei, W., Whitaker, F., Hoteit, H. and Vahrenkamp, V., 2021. The creation of calcite microcrystals and microporosity through deep burial basinal flow processes driven by plate margin obduction – a realistic model? *Marine and Petroleum Geology*, **136,** 105432, 20 pp.
Weissert, H., Lini, A., Follmi, K.B. and Kuhn, O., 1998. Correlation of Early Cretaceous carbon isotope stratigraphy and platform drowning events: a possible link? *Palaeogeography, Palaeoclimatology, Palaeoecology*, **137**, 189-203.
Weissert, H. and Erba, E., 2004. Volcanism, CO_2 and palaeoclimate: a Late Jurassic – Early Cretaceous carbon and oxygen isotope record. *Journ. Geol. Soc.* **161**, 695-702.
Wilson, J. L., 1967. Cyclic and reciprocal sedimentation in Virgilian strata of southern New Mexico. *Geol. Soc. Am. Bull.*, **78**, 805-818.
Wilson, J. L., 1975. Carbonate Facies in Geologic History. New York, Springer-Verlag, 471 pp.
Yamamoto, K., Ishibashi, M., Takayanagi, H., Asahara, Y., Sato, T., Nishi, H. and Iryu, Y., 2013. Early Aptian paleoenvironmental evolution of the Bab Basin at the southern Neo-Tethys margin: response to global carbon-cycle perturbations across Ocean Anoxic Event 1a. *Geochemistry Geophysics Geosystems*, **14**, 1104-1130.
Yamamoto, K., Ottinger, G., Al Zinati, O., Takayanagi, H., Yamamoto, K. and Iryu, Y., 2018. Geochemical, petrographical, and petrophysical evaluations of a heterogeneous, stratiform dolomite from a Barremian oil field, offshore Abu Dhabi (UAE). *AAPG Bull.*, **102,** 129-152.
Zhang, H.W., Sun, Y.Q., Li, Y., Zhou, X.D., Tang, X.Z., Yi, P., Murad, A., Hussein, S., Alshamsi, D., Aldahan, A., Yu, Z.B., Chen, X.G. and Mugwaneza, V.D.P., 2017. Quality assessment of groundwater from the south-eastern Arabian Peninsula. *Environmental Monitoring and Assessment*, DOI 10.1007/s10661-017-6092-2, 14 pp.
Zhang, S., and Lu, P., 2019. Effect of micrite content on calcite cementation in an Upper Jurassic carbonate reservoir, eastern Saudi Arabia. *Journal of Petroleum Geology*, **42**, 79-90.
Ziegler, M.A., 2001. Late Permian to Holocene paleofacies evolution of the Arabian Plate and its hydrocarbon occurrences. *GeoArabia*, **6** (3), 445-504.